Aiglon: A Particle Detector for Geophysics on board the China Seismological Experiment Satellite

W.J. Burger
Università degli Studi di Perugia

18.09.2013 – Laboratori Nazionali di Frascati

I Background

Ionospheric Precursor Phenomena and Particle Precipitation from the Inner Radiation Belts

II The High Energy Particle Detector Aiglon

Design Considerations, Expected Performance, Current Status

III Simulation Model

Interpret Precipitation Data, Optimise Detector Design

Precursor Phenomena in the Earthquake Preparation Zone

- Increase of the local Radon concentration (^{222} Rn, α emitter, half-life 3.8 d) $\Rightarrow$ local ionisation
- Important gas discharges including volatile metallic aerosols (Hg, As, Sb)
- Formation of heavy molecular ion clusters $H_3O^+ \cdot (H_2O)_m$, $HNO_3^- \cdot (H_2O)_m$, $NO_3^- \cdot (HNO_3)_n (H_2O)_m$

$\Rightarrow$ Anomalously Large Vertical Electrical Field

Electric Field Variations Prior to Strong Earthquakes

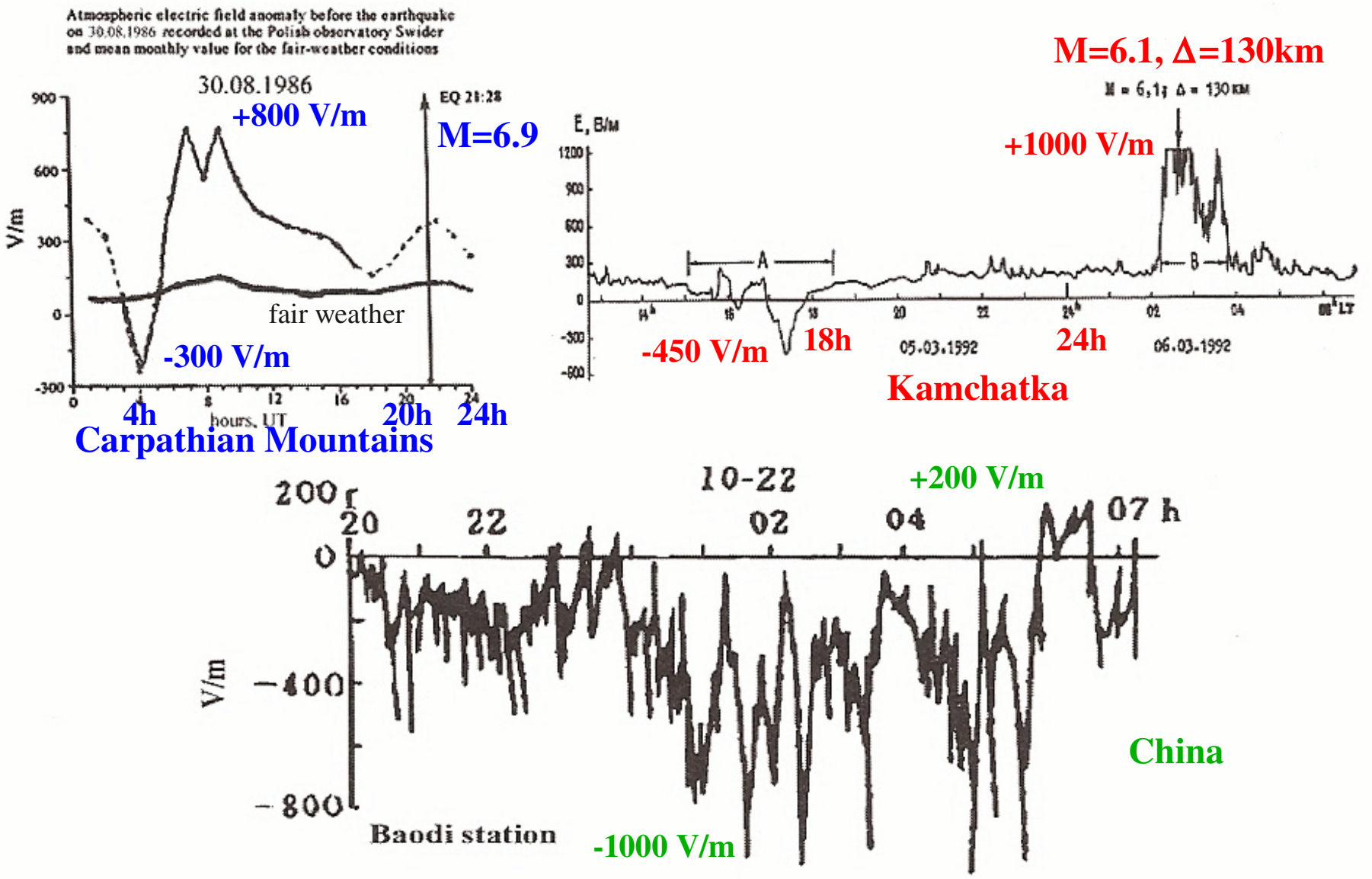

Fig. 1.10 Examples of anomalous electric field registration before strong earthquakes (Nikiforova and Michnowski 1995; Vershinin et al. 1999; Hao et al. 2000)

Sergey Pulinets
Kirill Boyarchuk
Springer 2004

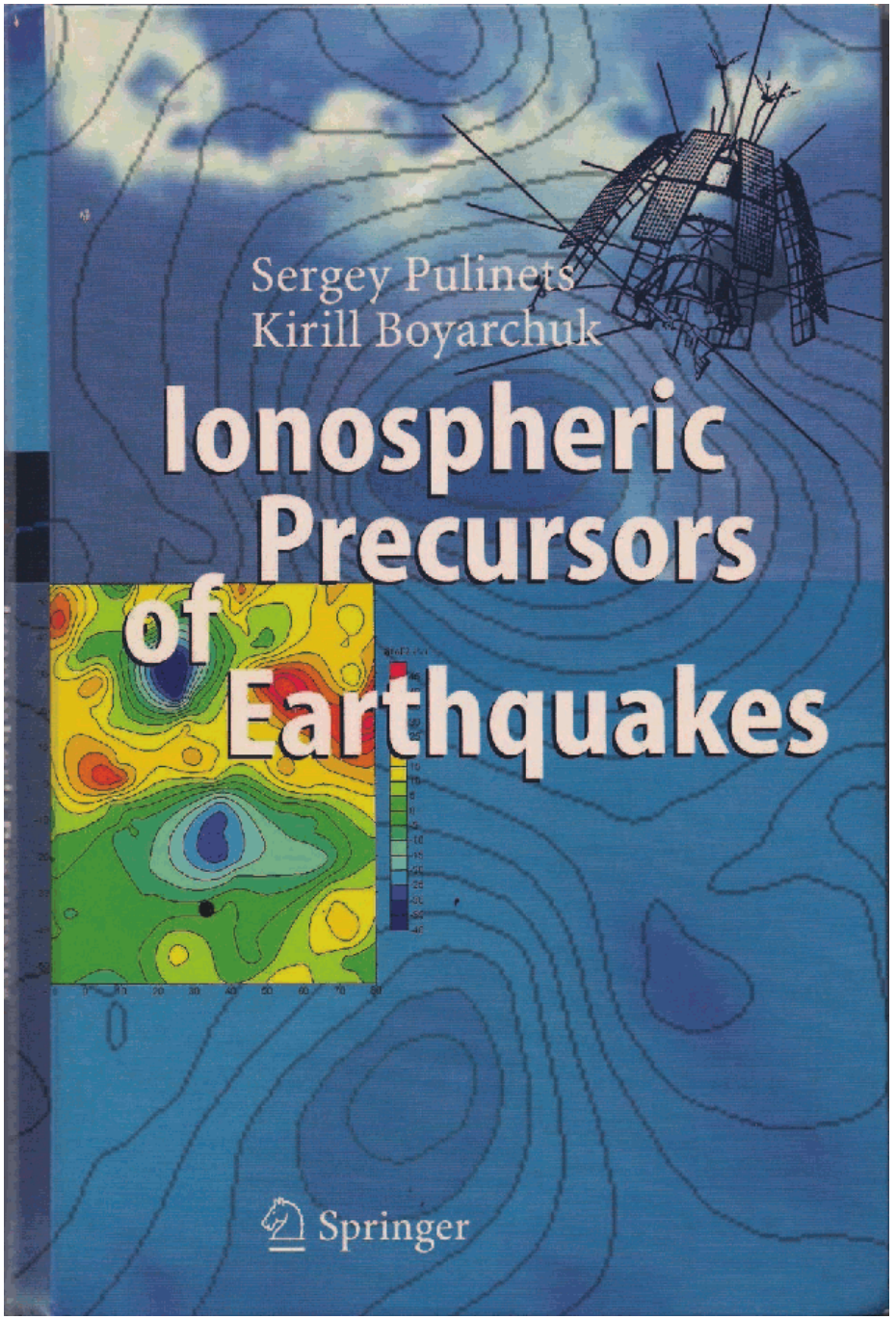

The Lithosphere.Atmosphere-Ionosphere Coupling Model

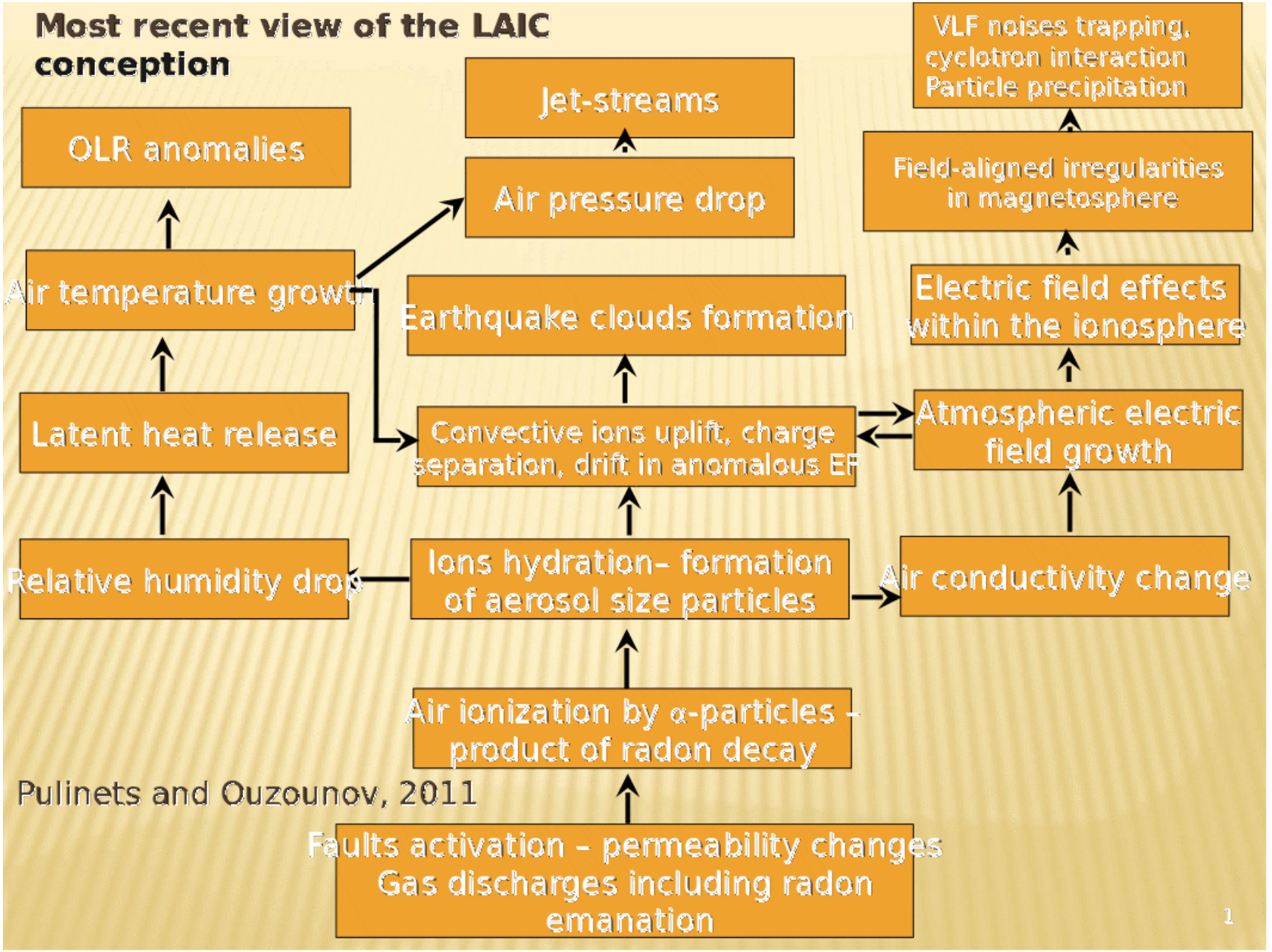

Ionosondes (1-20 MHz) Sample the Electron Density

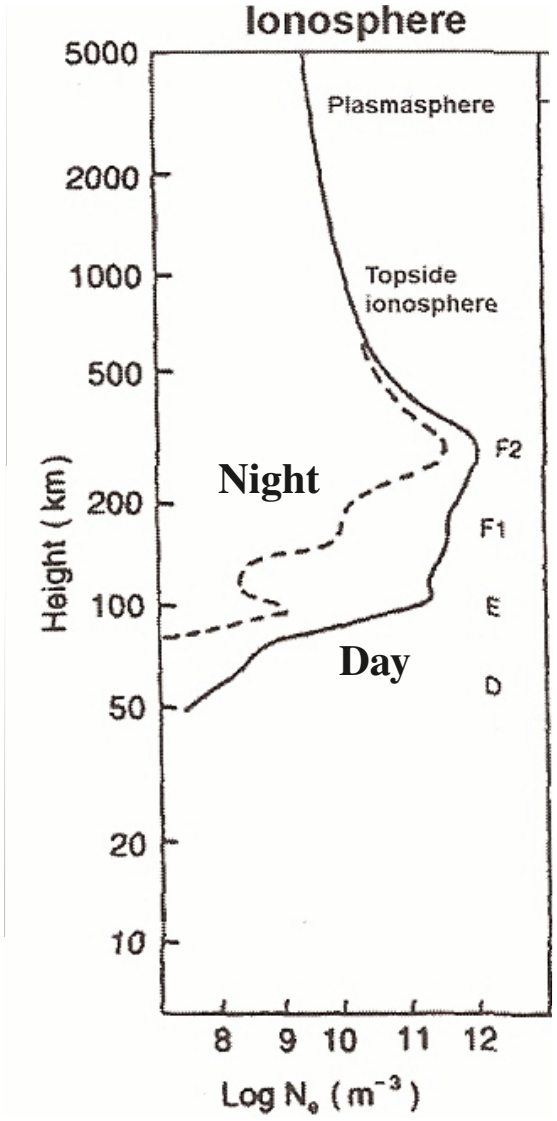

The electromagnetic radiation emitted with a frequency lower than the plasma frequency is reflected .

Plasma frequency

$$\omega_p = \left(\frac{4\pi n_e e^2}{m_e} \right)^{1/2} \quad \text{rad/s}$$

Ordinary wave

$$f_o \approx 8.98 \sqrt{n_e} \quad \text{Hz} \qquad n_e \text{ in m}^{-3}$$

Critical frequency

$$f_o F2 \approx 8.98 \sqrt{n_{max}} \quad \text{Hz}$$

Above the critical frequency the ionsphere is transparent for the emitted radiation.

Ionospheric Precursors Observed by Ground Ionosondes

$$\Delta f_0F2(\%) = (f_0F2_{cur} - f_0F2_{ref}) \times 100 / f_0F2_{ref}$$

$$\Delta f_0F2(MHz) = (f_0F2_{cur} - f_0F2_{ref})$$

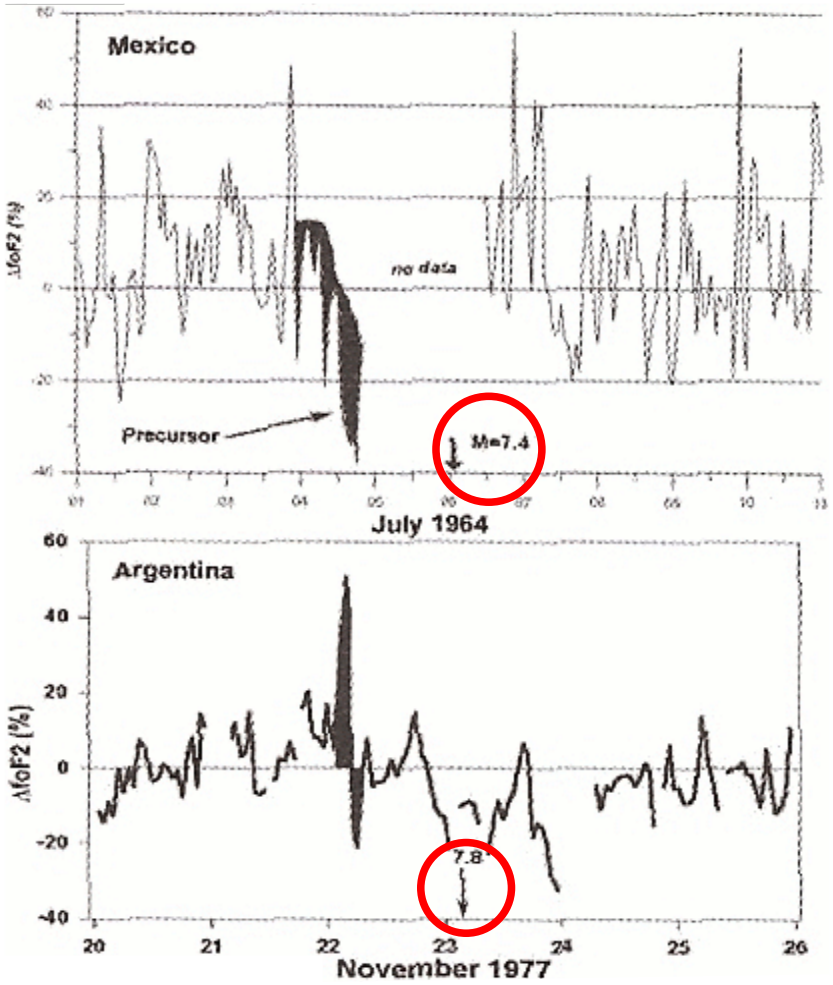

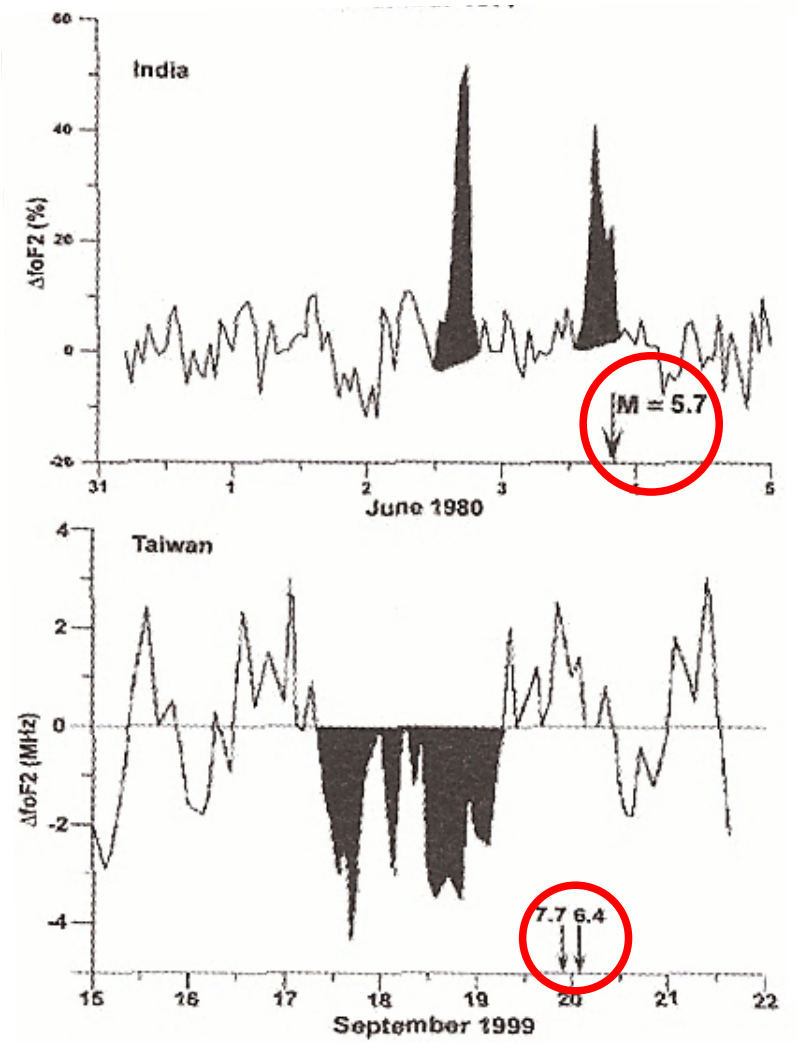

Ionospheric Precursors Observed by Satellites

1980 New Guinea Earthquake M = 7.3

Intercosmos-19

Δt = -48 h

Δt = -24 h

Δt = +24 h

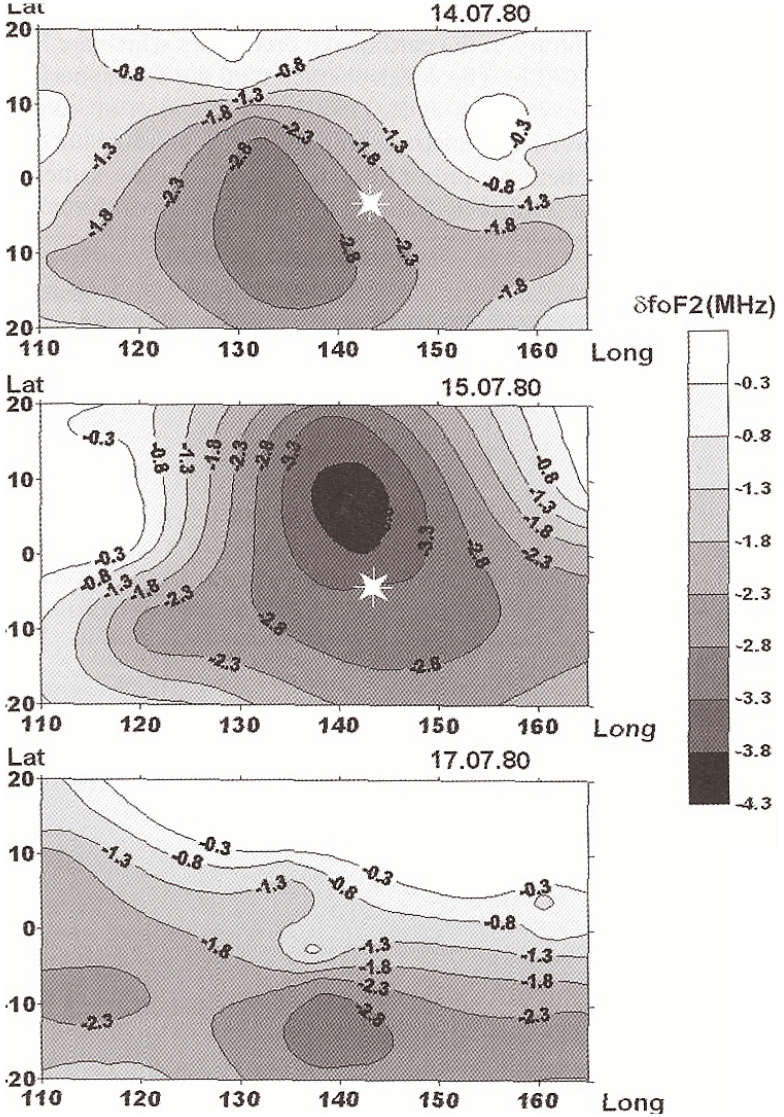

1964 Alaska Earthquake M = 9.2

Alouette-1 and ground ionosondes

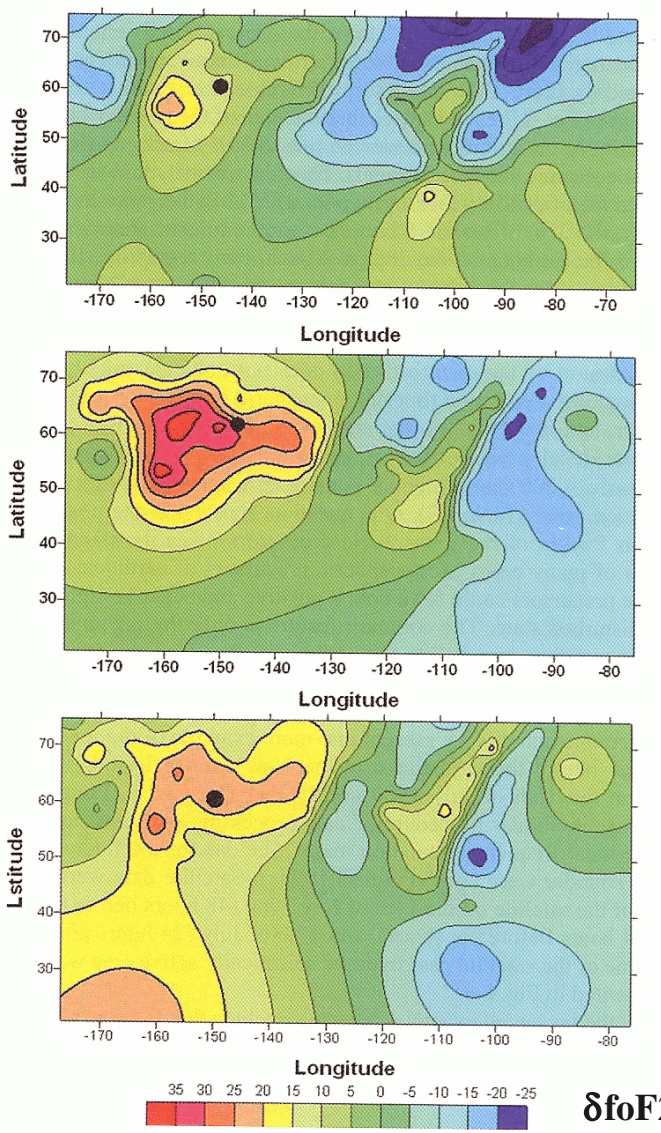

Total Electron Content (TEC) from GPS

The observed modulation of the traveling time and direction of the signals (GHz) are sensitive to the electron density.

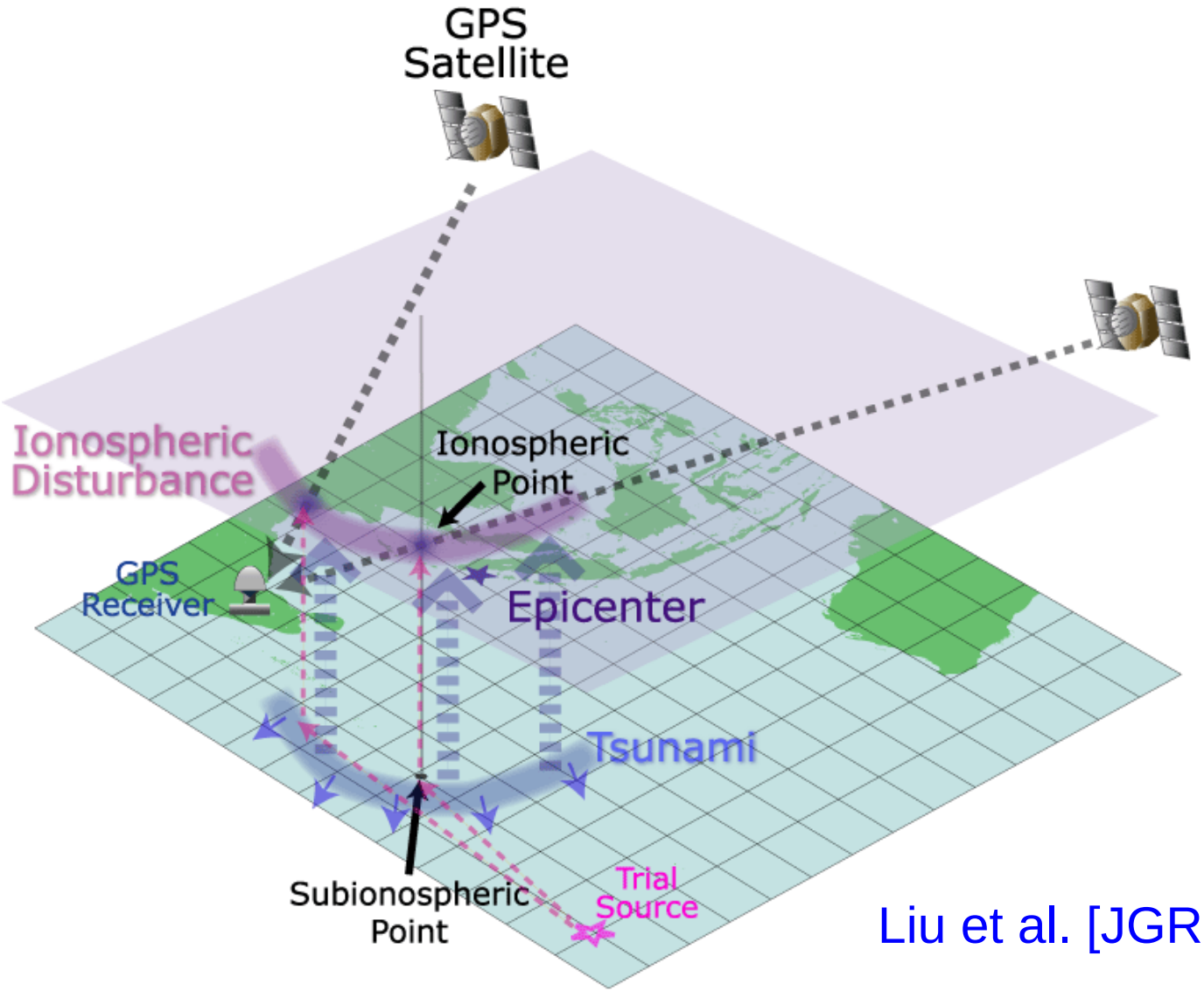

Liu et al. [JGR, 2006]

Variation of TEC observed on March 11, 2011 (M9 Tohoku Earthquake)

Liu et al. (JGR 2011)

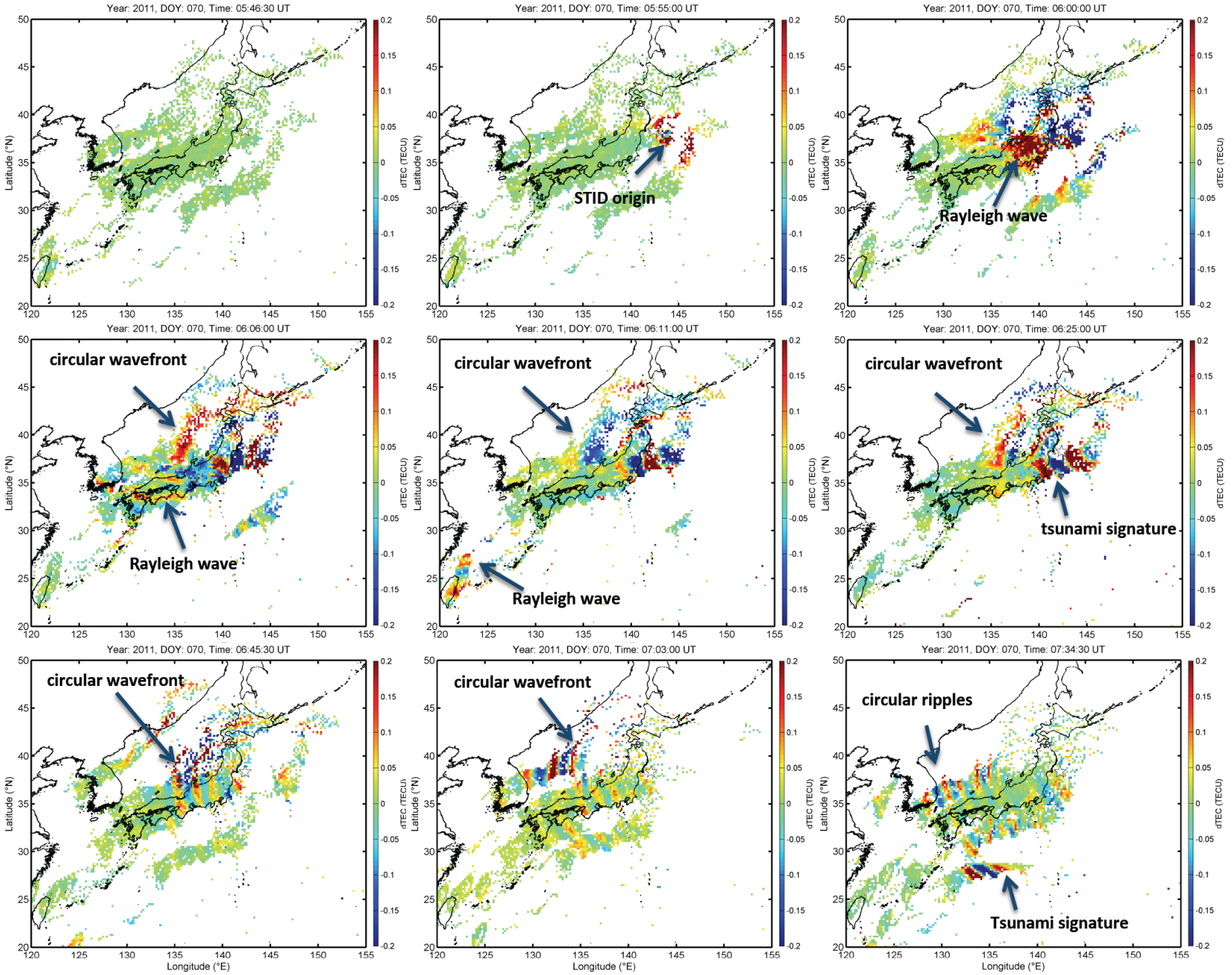

Particle Precipitation from the Inner Radiation Belts

S.Yu. Aleksandrin et al., Annales Geophysicae 21 (2009) 597

M > 4, |ΔL| < 0.1

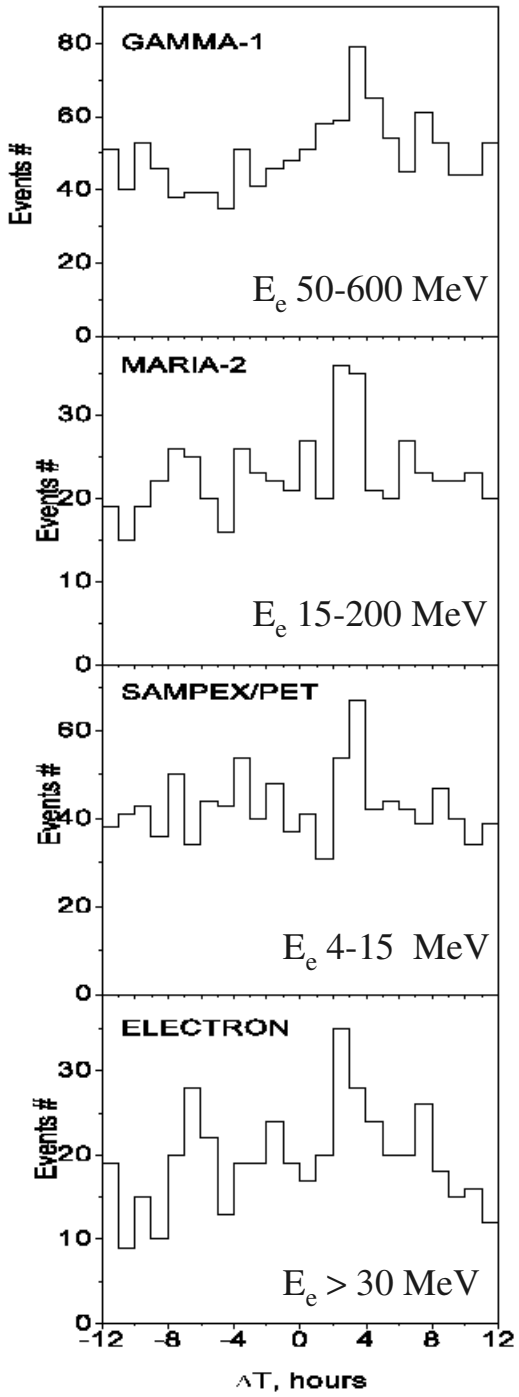

⇒

M > 5, |ΔL| < 0.07

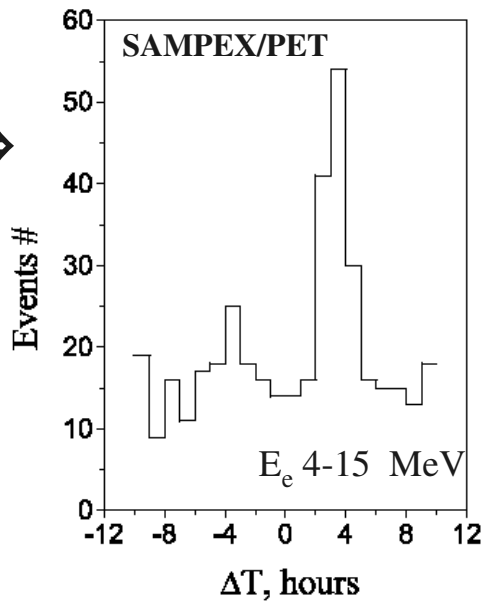

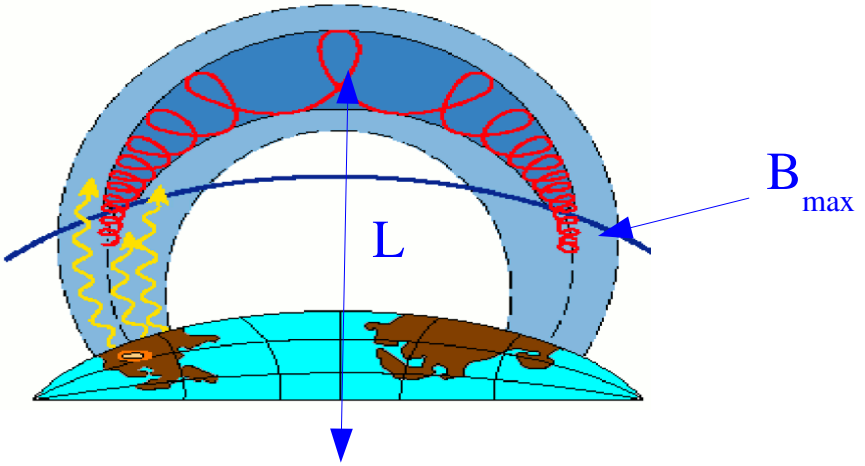

Drift Shell Variables

L, B_{max}

$\Delta T = T_{EQ} - T_{PB}$

$\Delta L = L_{EQ} - L_{PB}$

L_{EQ} = L coordinate at an altitude of 300 km above the epicenter

ARINA

A.M. Galper, Erice, Italy, 23 October 2012

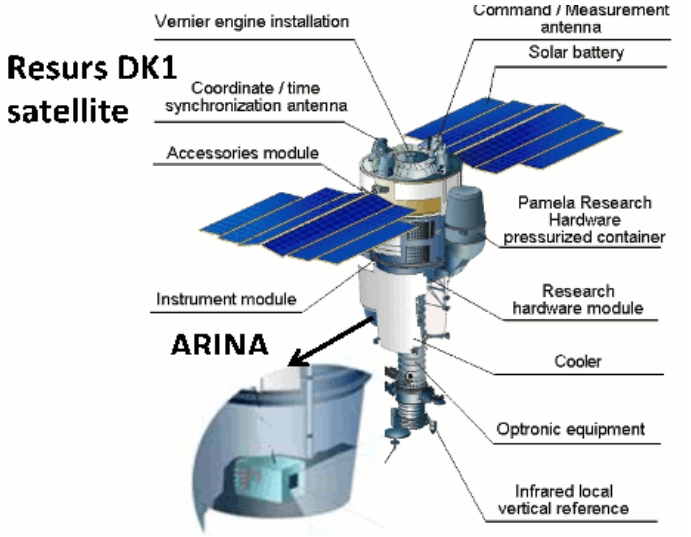

Event 29.05.2012 M = 4.3-5.5 ΔT = 1.0h

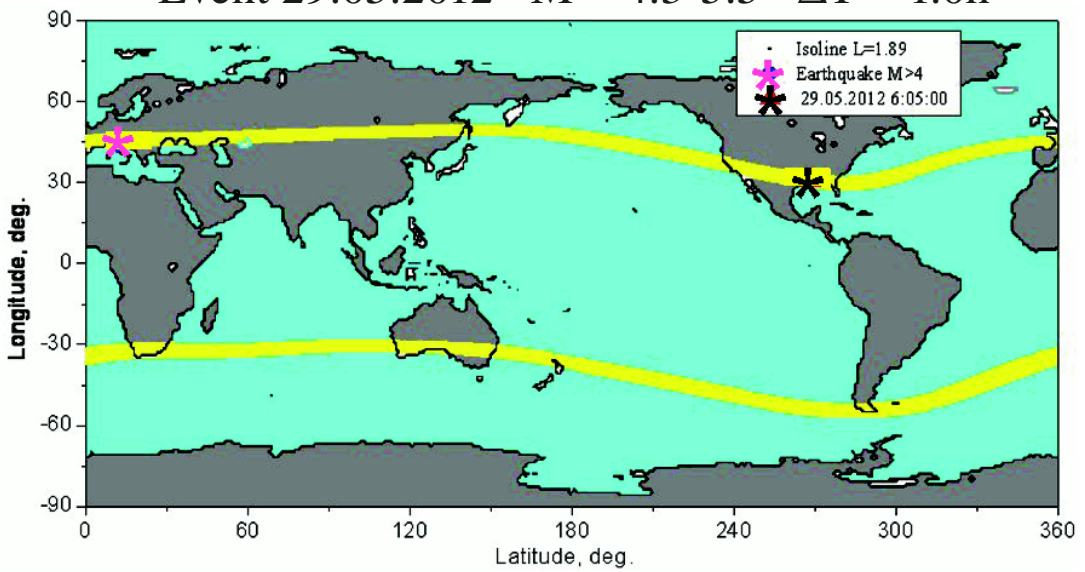

M > 4, |ΔL| < 0.1

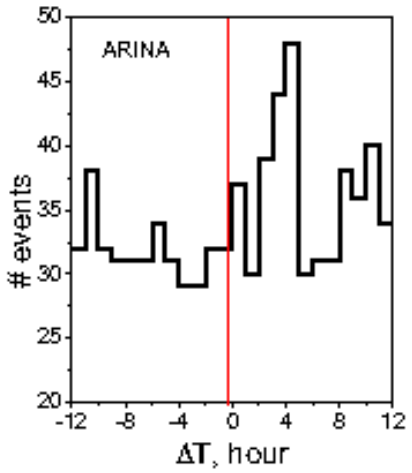

Event 29.02.2012 M = 5.0 ΔT = 2.2h

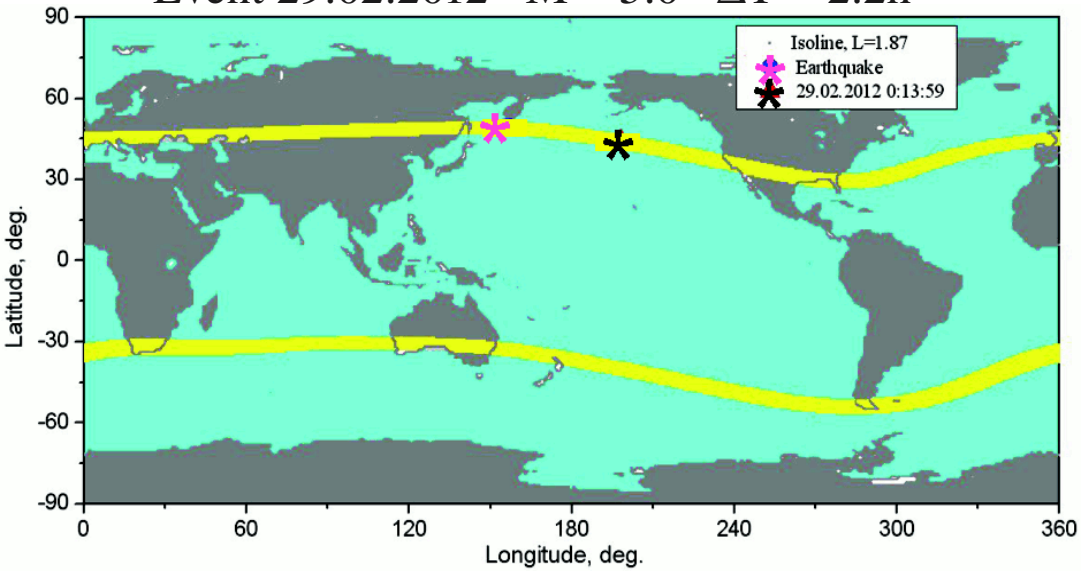

NOAA Polar Orbit Environment Satellites

R. Battiston, V. Vitale

300 keV electrons, M > 5, $|\Delta L| < 0.1$, L_{EQ} (900 km)

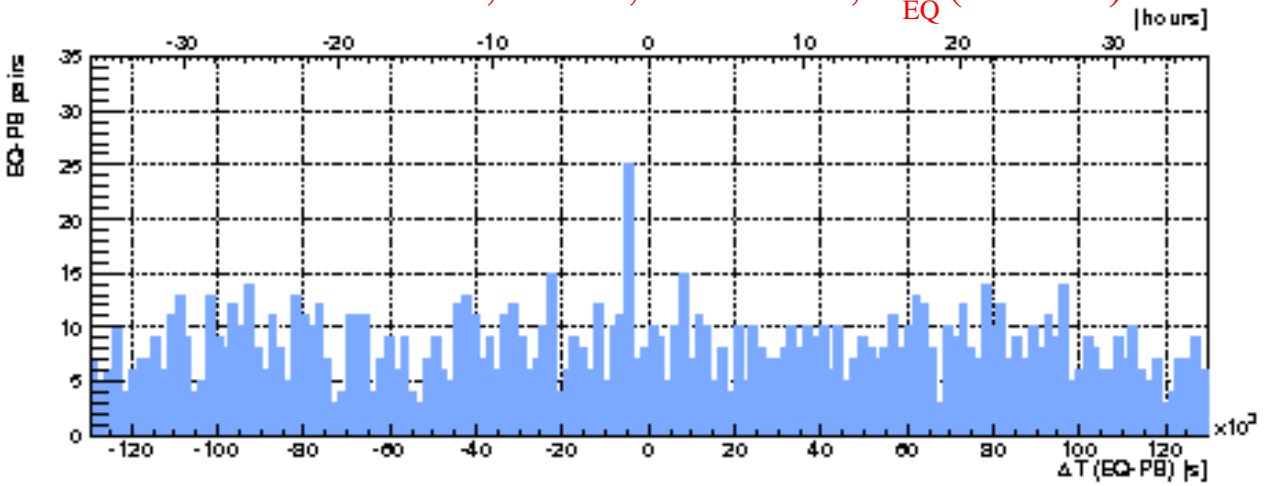

$\Delta T = -1.25 \pm 0.25$ h

PB - EQ

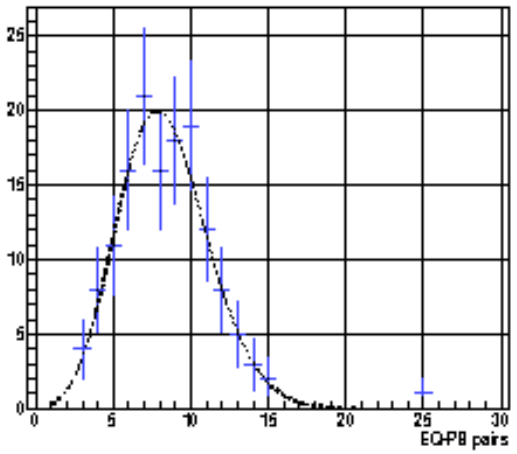

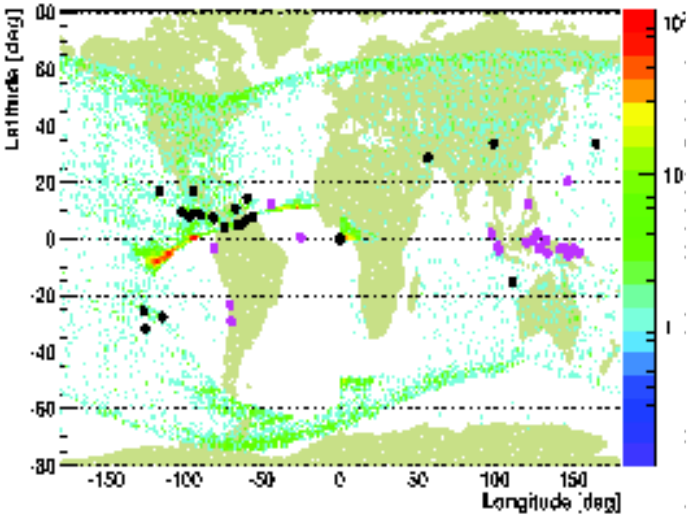

Plasma Analyser

Electric sensor

Electronic module

Energetic Particle Analyser

Magnetic sensors

Langmuir probe

Conclusions

We have statistically shown that there are ionospheric perturbations prior to EQs during night time.

- No wave perturbation
- Density perturbations at the altitude of the satellite and at the bottom of the ionosphere

DEMETER IDP

J.A. Sauvaud et al., Planetary and Space Science 54 (2006) 502-511

Observed particle precipitation of the inner radiation belt electrons due to the VLF electromagnetic radiation of ground emitters in the range 10-100 kHz.

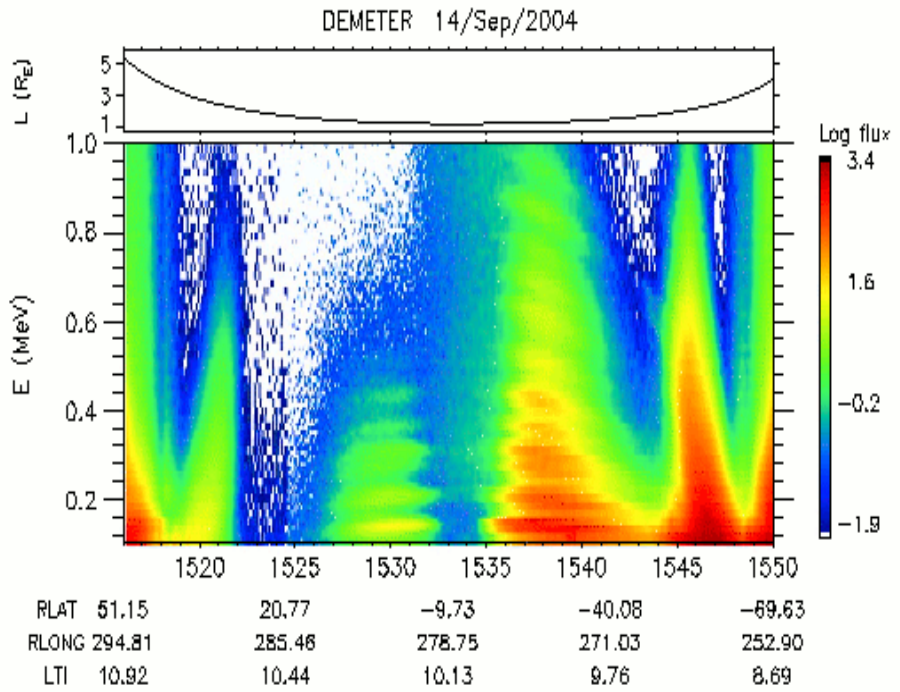

Fig. 9. Energy time spectrogram of electrons between 0.1 and 2 MeV taken just West of the South Atlantic Anomaly (SAA) on September 14, 200 top panel illustrates the variation of the *L* value of the satellite.

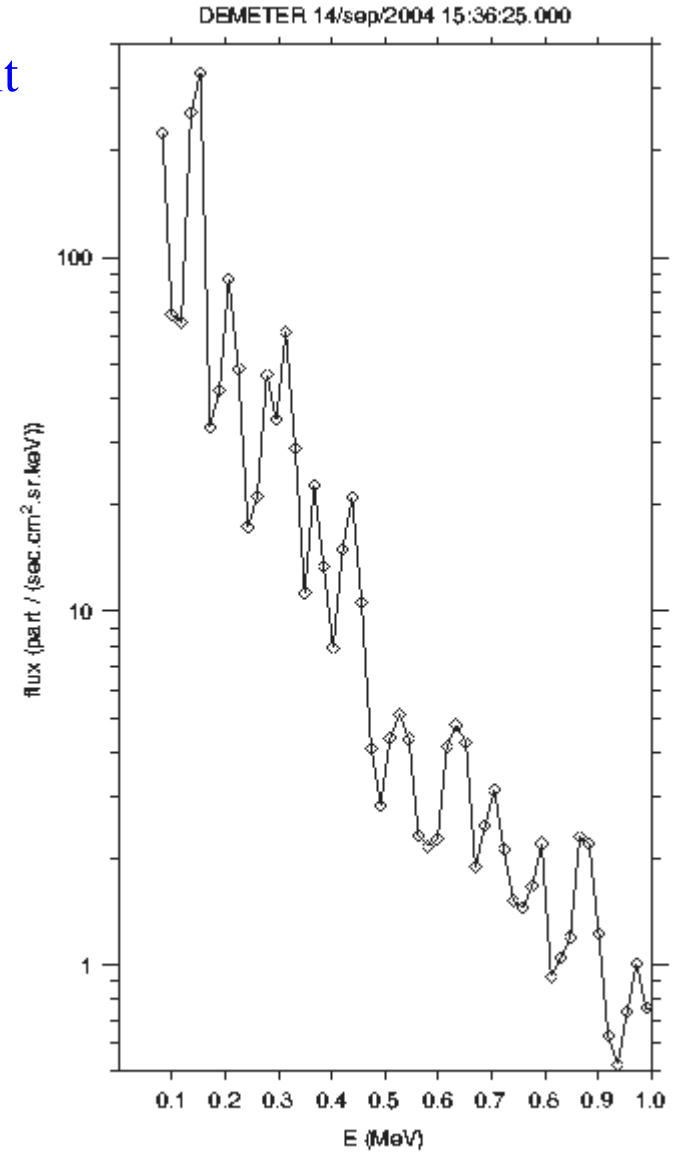

Fig. 10. Electron energy spectrum corresponding to Fig. 9 at 1536:33 UT. Note the succession of peaks from 150 keV up to ~1 MeV.

Energy resolution $< 8\%$

DEMETER observations of transmitter-induced precipitation of inner radiation belt electrons

K.L. Graf et al., Journal of Geophysical Research Vol. 114 (2009) A07205

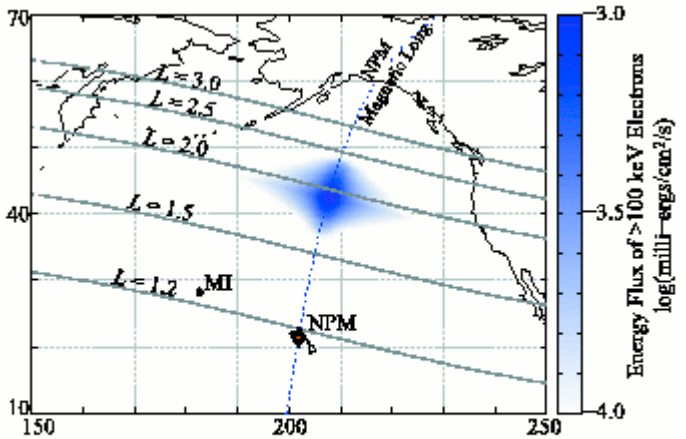

Figure 1. Location and magnitude of predicted NPM-induced precipitation region with the locations of the NPM transmitter and Midway Island (MI) receiver marked.

Table 1. Results of Analyzing the 194 DEMETER Passes When NPM was Transmitting in a 5-sec ON/5-sec OFF Format for NPM-Correlated Bursts of Energetic Particle Flux

	Number of Occurrences in Precipitation Region	Number of Occurrences in Conjugate Region
2 Correlated bursts	3	2
1 Correlated burst	9	13
No bursts detected	73	82
1 Uncorrelated burst	5	6
2 Uncorrelated bursts	1	0
Total number of passes	91	103

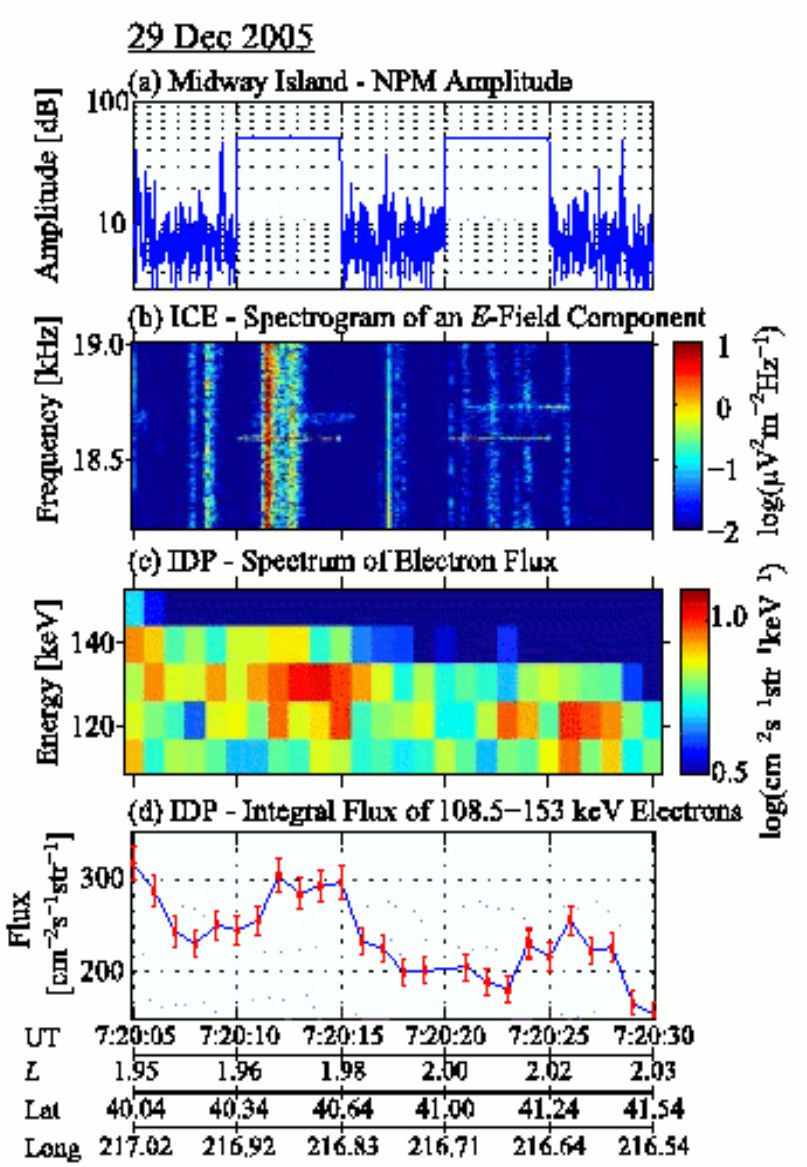

Sensor Web Approach for Earthquake Early Warnings

D. Ouzounov. Erice, Oct. 22, 2012

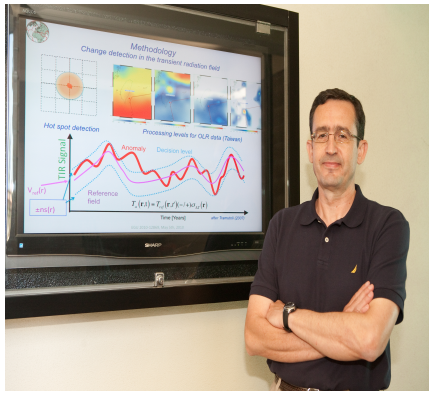

Dimitar Ouzounov,
Chapman Univ, USA

Sergey Pulinets
IAG, Russia

Katsumi Hattori
Chiba Univ, Japan

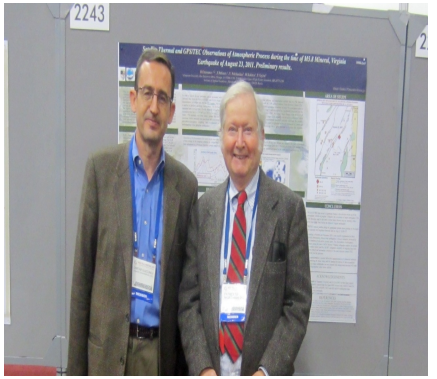

Patrick Taylor
NASA/GSFC, USA

Chapman Menas
Kafatos, Univ, USA

Valerio Tramutoli
Basilicata Uni, Italy

Michel Parrot
LPC2E/CNR, *France*

J.Y.Liu (Tiger),
NCU, Taiwan

Email Notification:
On Mon, Oct 11, 2010 at 8:27 AM, <
dimitar.p.ouzounov@nasa.gov> wrote:
Dear Shan,
The region I see currently from satellite with abnormal
activities is part of WC of Sumatra.
2S-4S/101E-103E
Regards,
Dimitar

On Tue, Oct 26, 2010 at 8:35 AM, <vu2rss@gmail.com> wrote:

dear sir, you still remember me?
I live in southern Sumatra, Thank you for your Prediction !!
tsunami disaster. after the earthquake last night ..400 people
were killed.
My brother survived, I warn him, because I have seen on your
site.
Thanks
Deri Kurnia

Erice, 21-24 ottobre 2012

China Seismological Experiment Satellite (CSES)

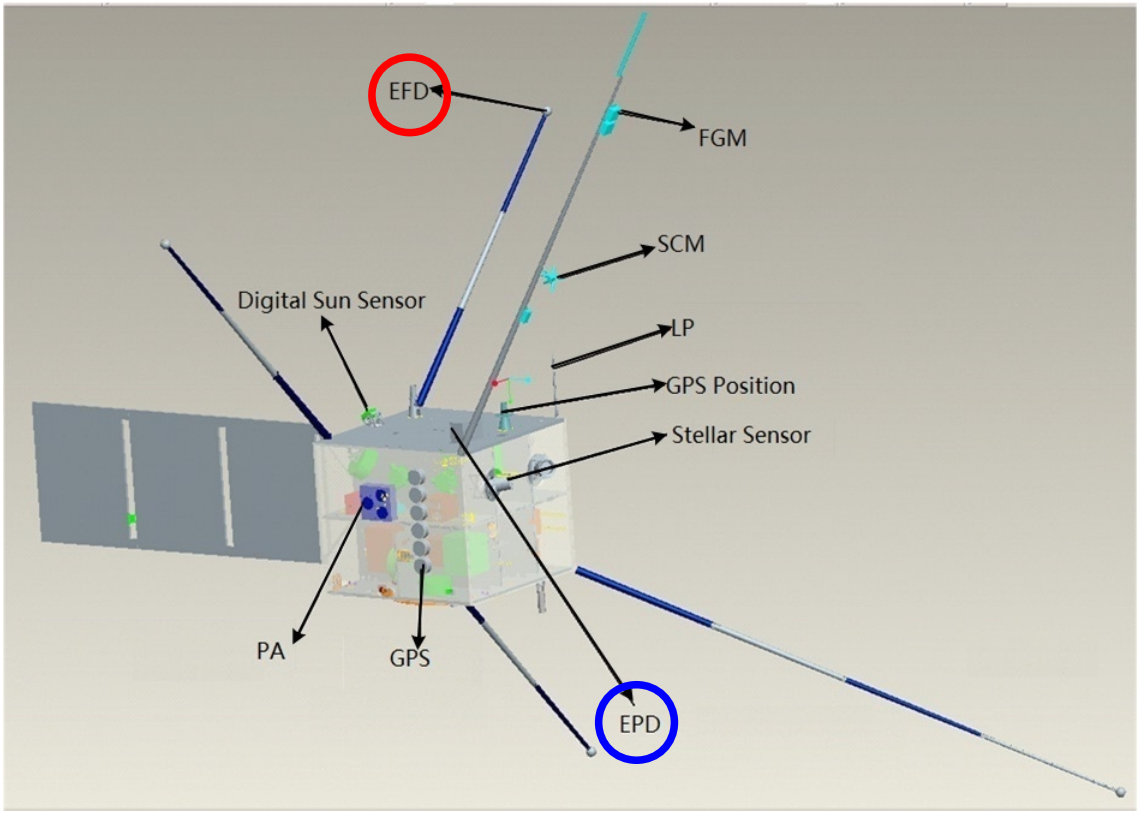

Electric Field Detector (INFN-Roma Tor Vergata, INFN-Roma3, CISAS-Padova)

Energetic Particle Detectors: Low Energy, 0.1-10 MeV electrons (LEPD)
(Institue of High Energy Phyiscs, CAS)
High Energy, 5-50 MeV electrons (*Aiglon* / HEPD)
(INFN-Bologna, INFN-Perugia)

The High Energy Particle Detector

The particle detector should measure low energy

electrons (< 50 MeV) and **protons (< 500 MeV)**

with best possible **angular** and **energy resolutions**, and with a sufficiently **large acceptance** to detect **short-term time** variations.

Magnetic Spectrometer

522 G NdFeB cylindrical magnet

∅ 13.8 cm, length 18.3 cm, FOV 37°

TOF scintillator planes

Si μstrip sensor planes

Si "edge-less" sensor filter planes

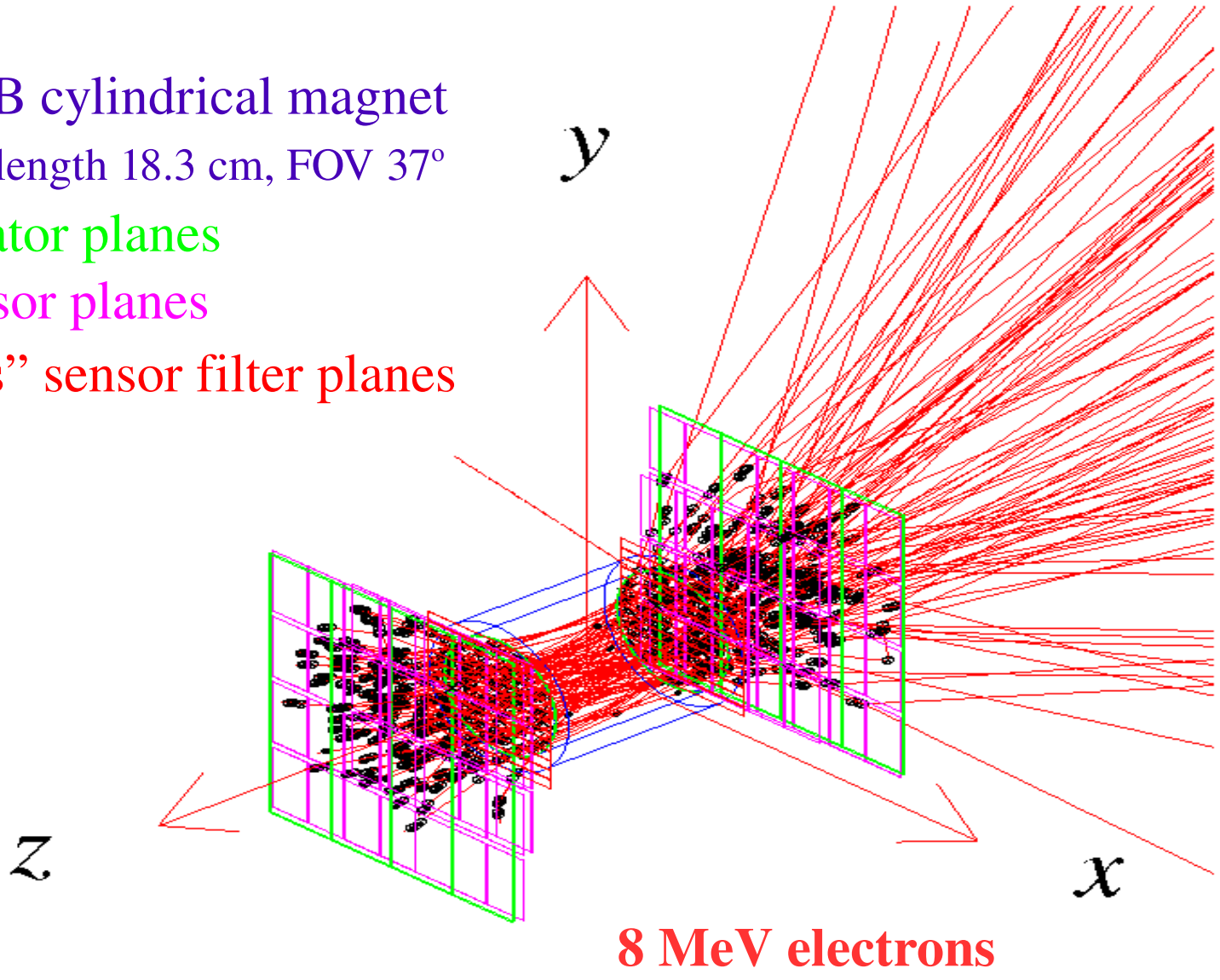

8 MeV electrons

$\mathbf{B} = B_o\mathbf{x}$

Filter Plane Parameters

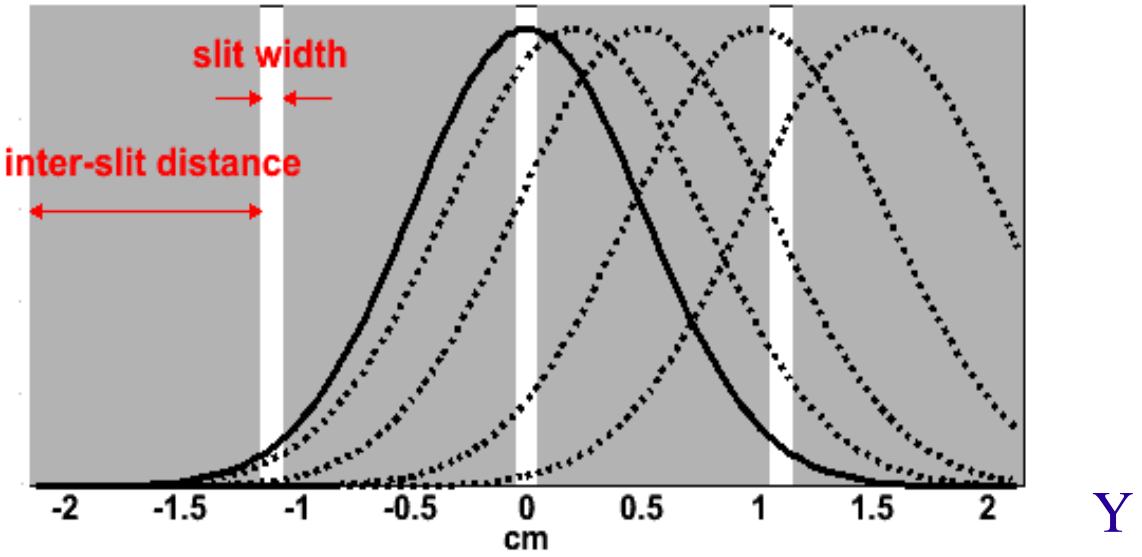

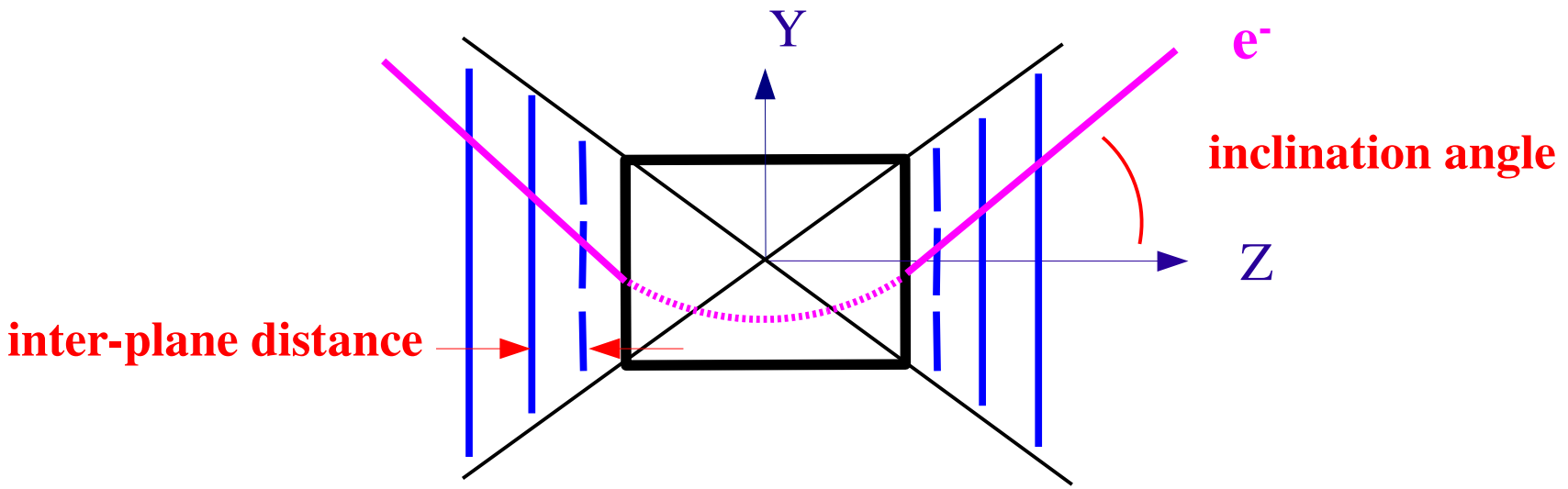

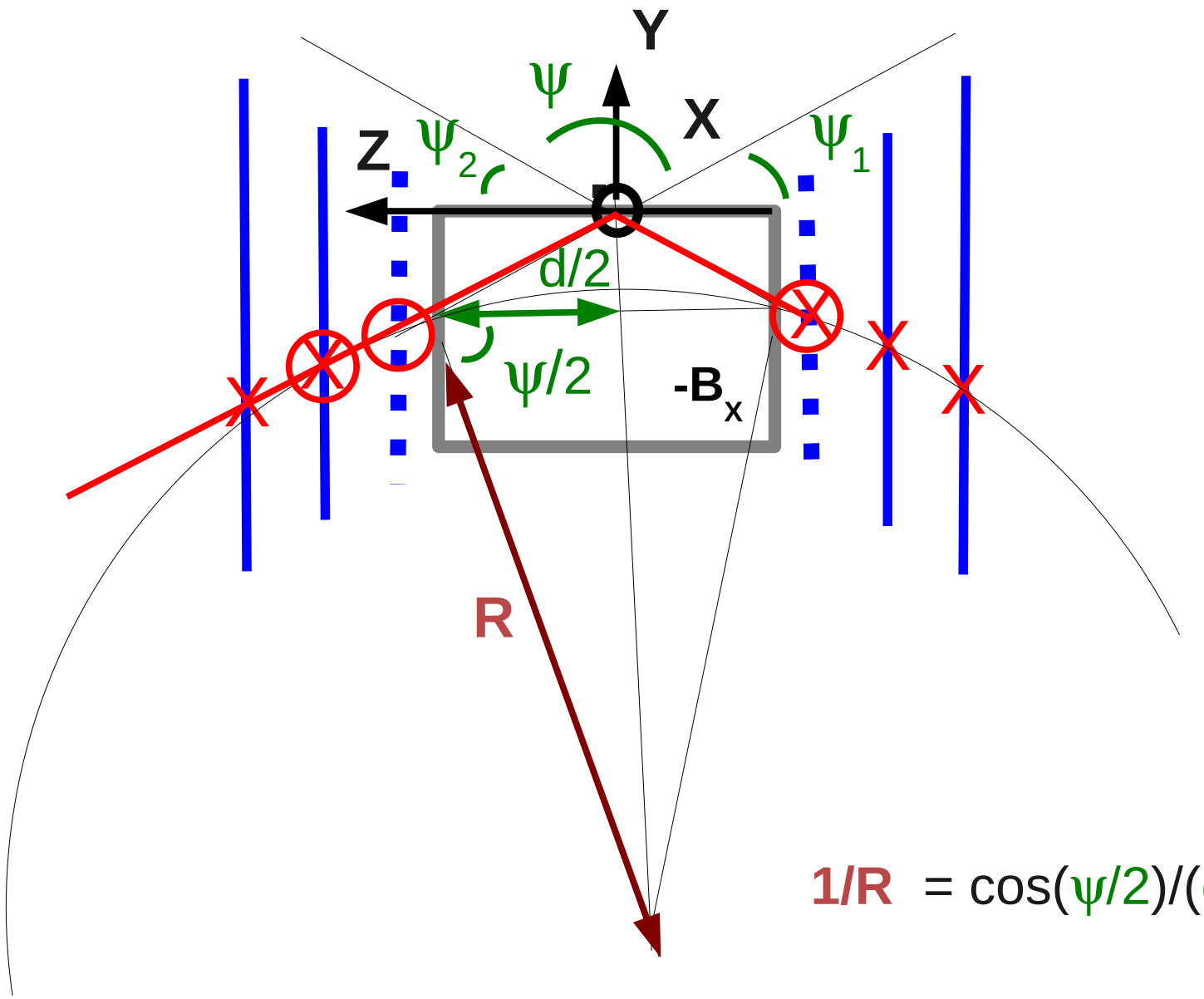

$1/R = \cos(\psi/2)/(d/2)$

1 Slit Event 3 point reconstruction

Electron Rigidity Resolution and Acceptance

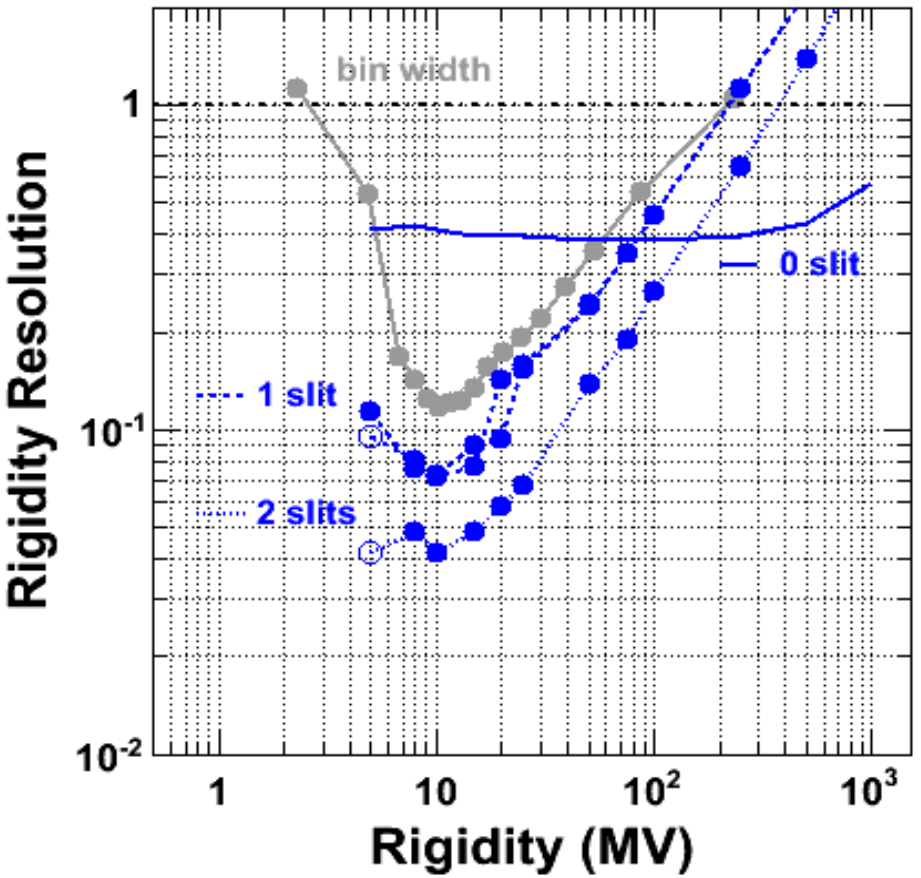

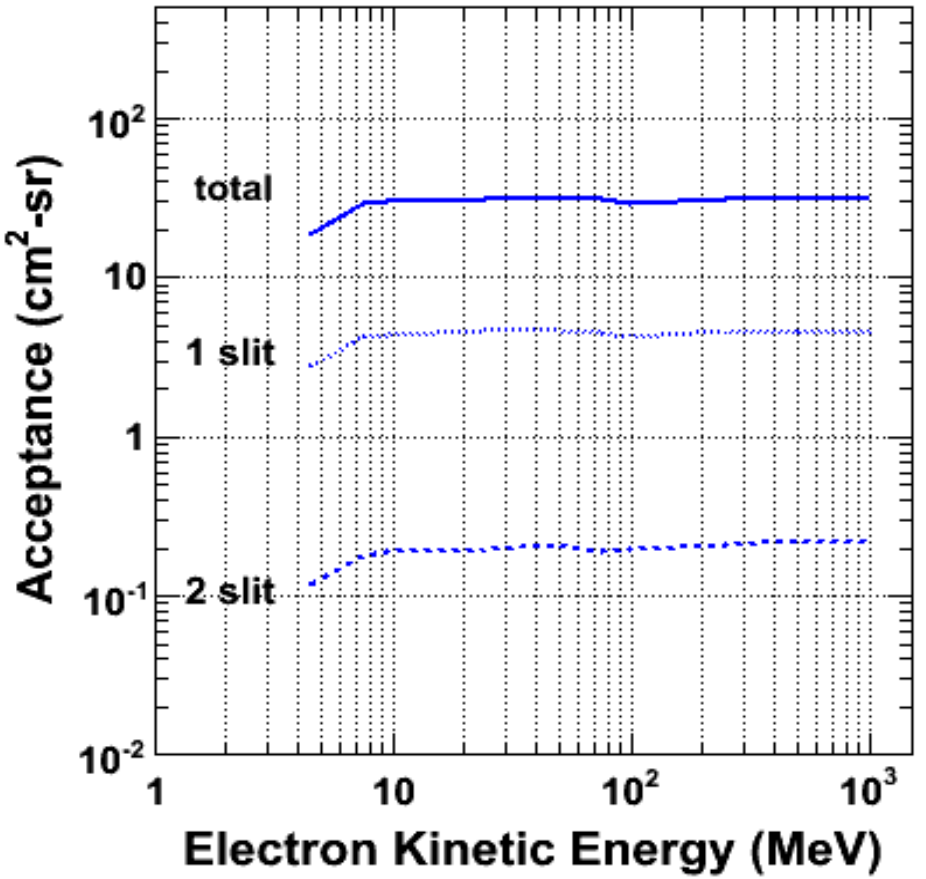

Rigidity Resolution for Downstream Slit Events

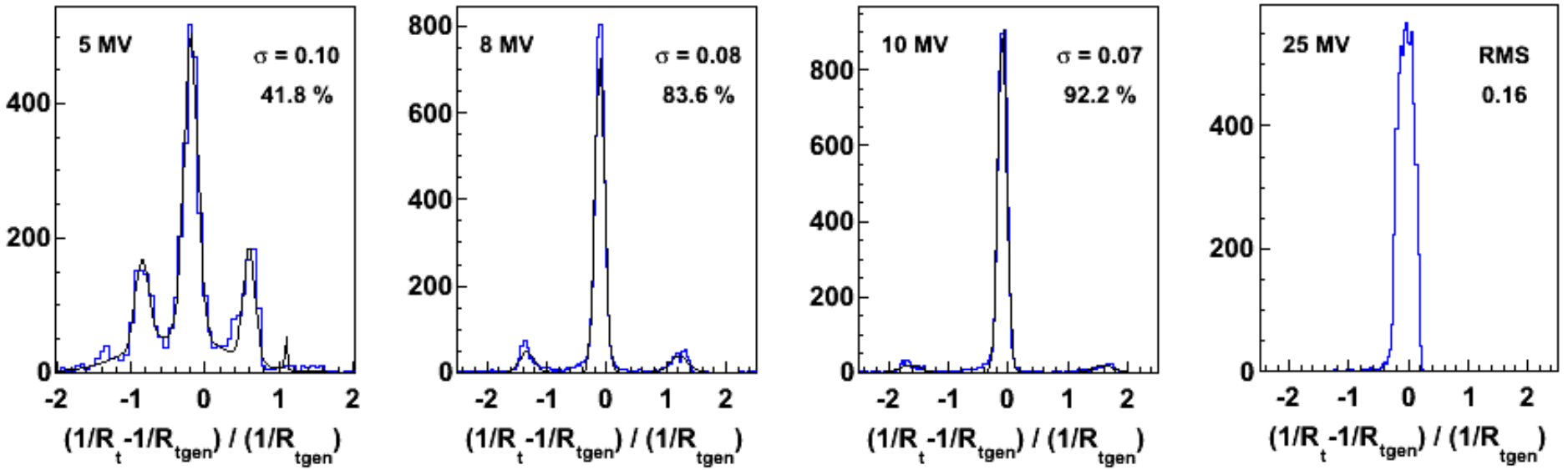

Reconstructed vs Generated (αE^{-3}) Rigidity Distributions

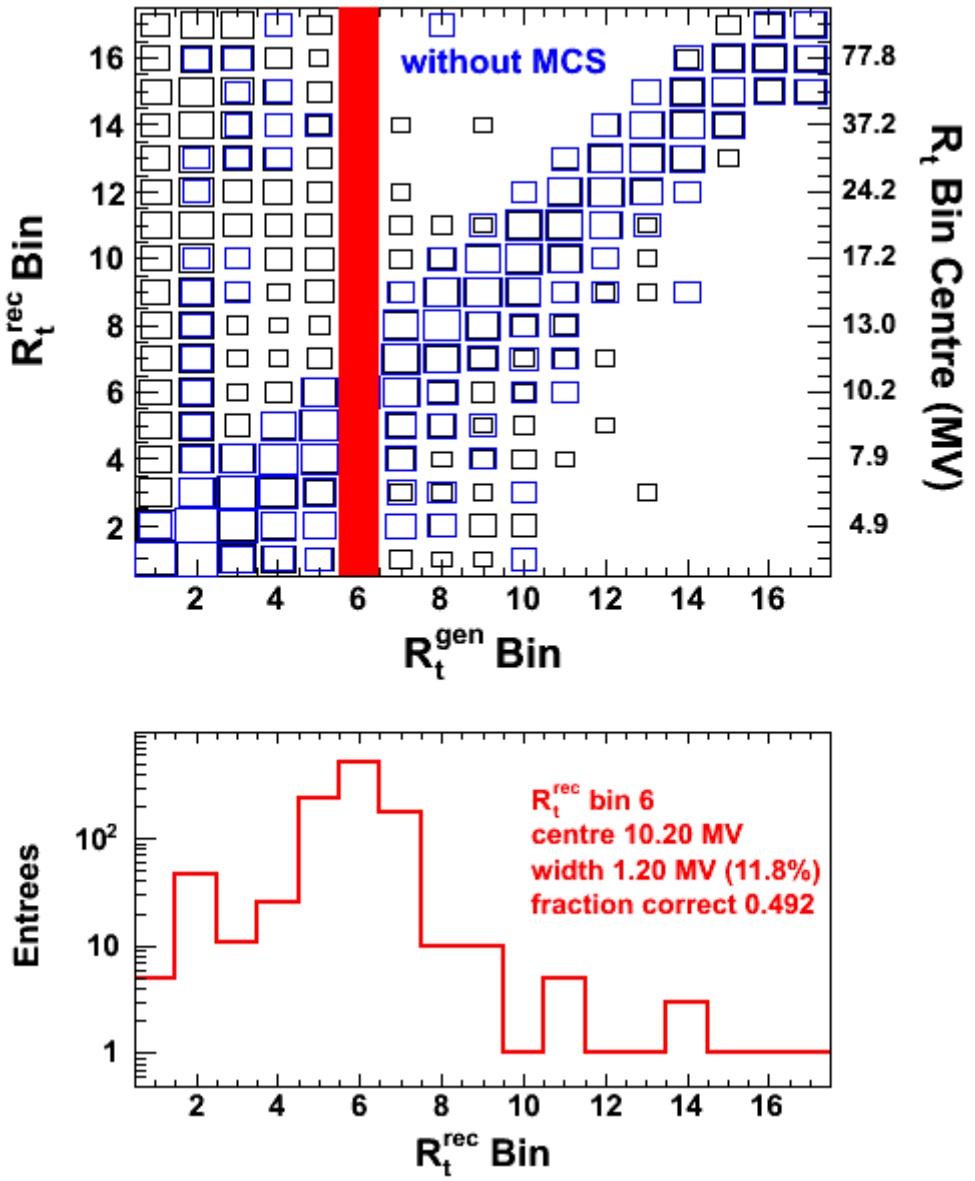

Angular Resolution

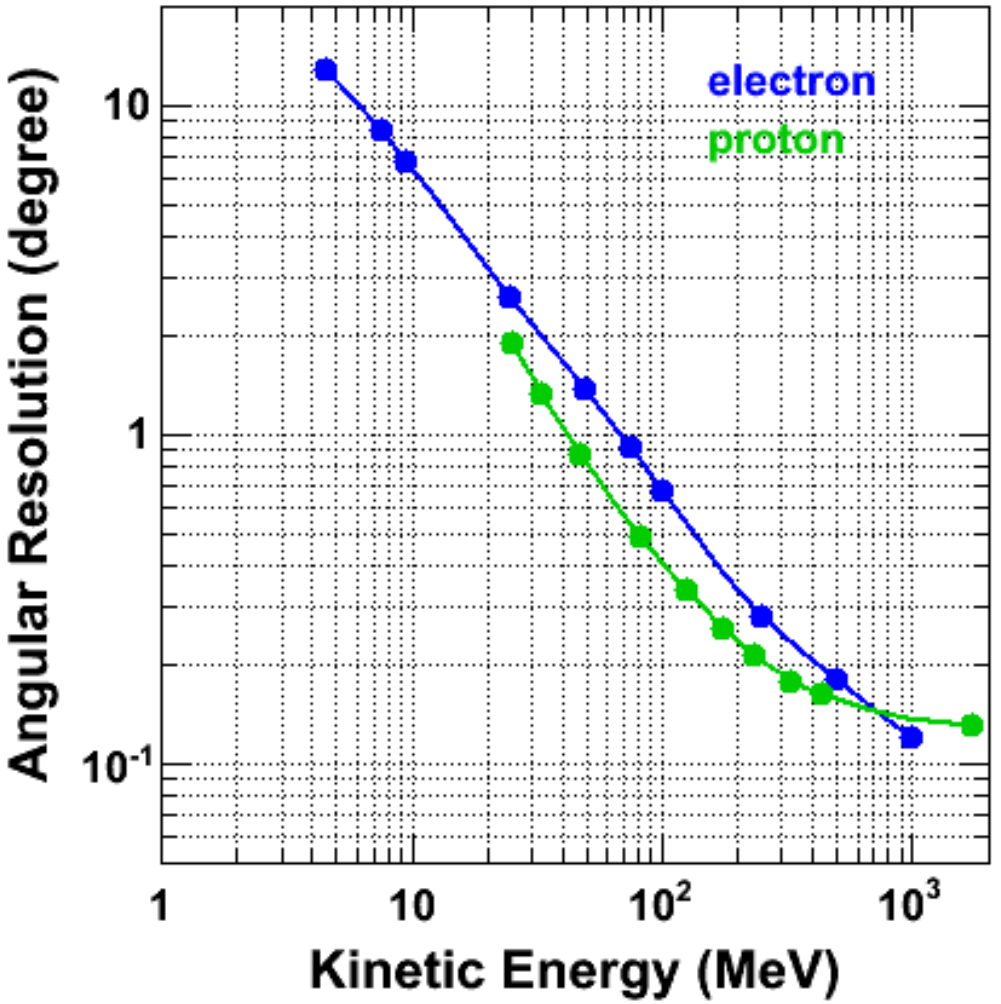

TOF provides the **proton energy** (left) and and **particle identification** (right)

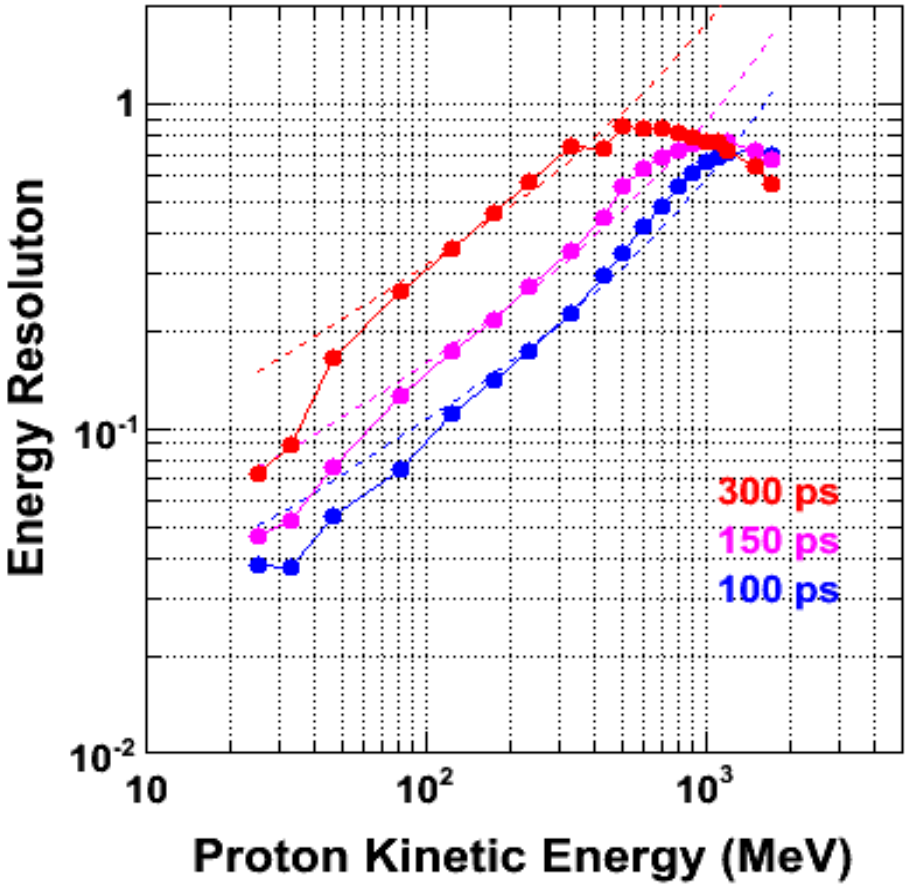

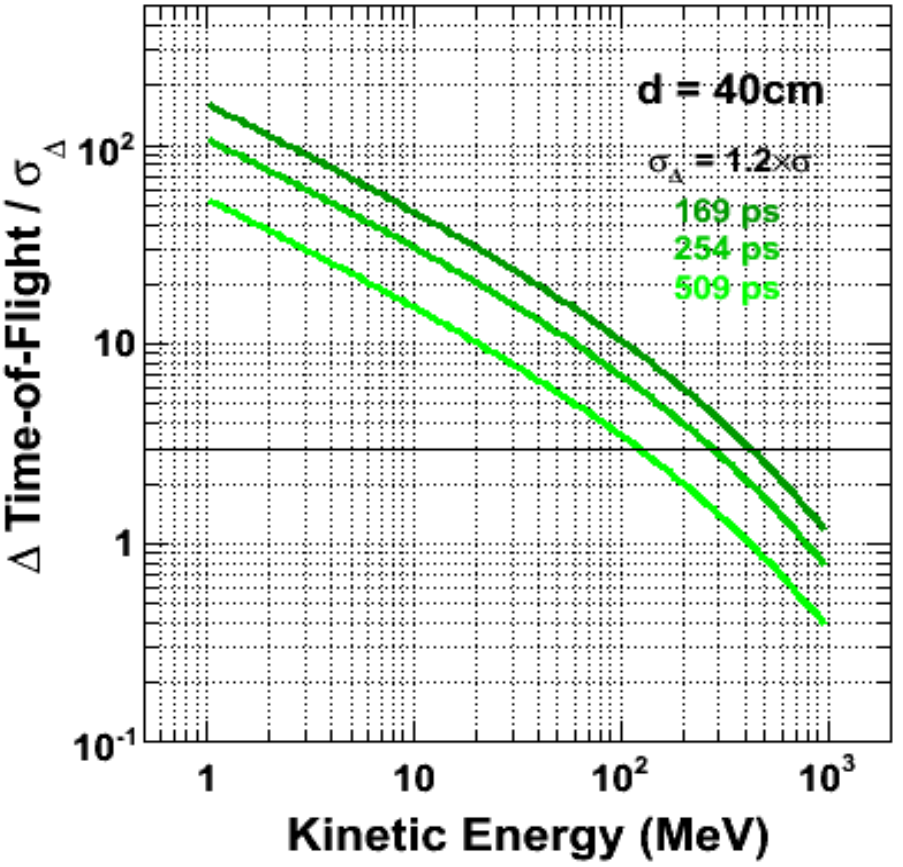

Performance Compared with Existing Satellite Particle Detectors.

Detector	Geometric Factor cm^2-sr	Aperture	Pitch Angle	Energy Range *MeV* Electron	Proton
SAMPEX PET	1.7	58°	0-90°	1-4 4-20	19-28 28-64
DEMETER IDP	1.2	32°	90°	0.07-2.4	
NOAA MEPED	0.01	30°	0°-90° 90°-0°	0.03-2.5	0.03-6.9
AIGLON	4.3 30	70^0	$0\text{-}90^0$	5-50	30-300
		Δ(12.5°-1.0°)	Δ(2.0°-0.2°)		

Mechanical Design

INFN Bologna
C. Guandalini
G. Laurenti

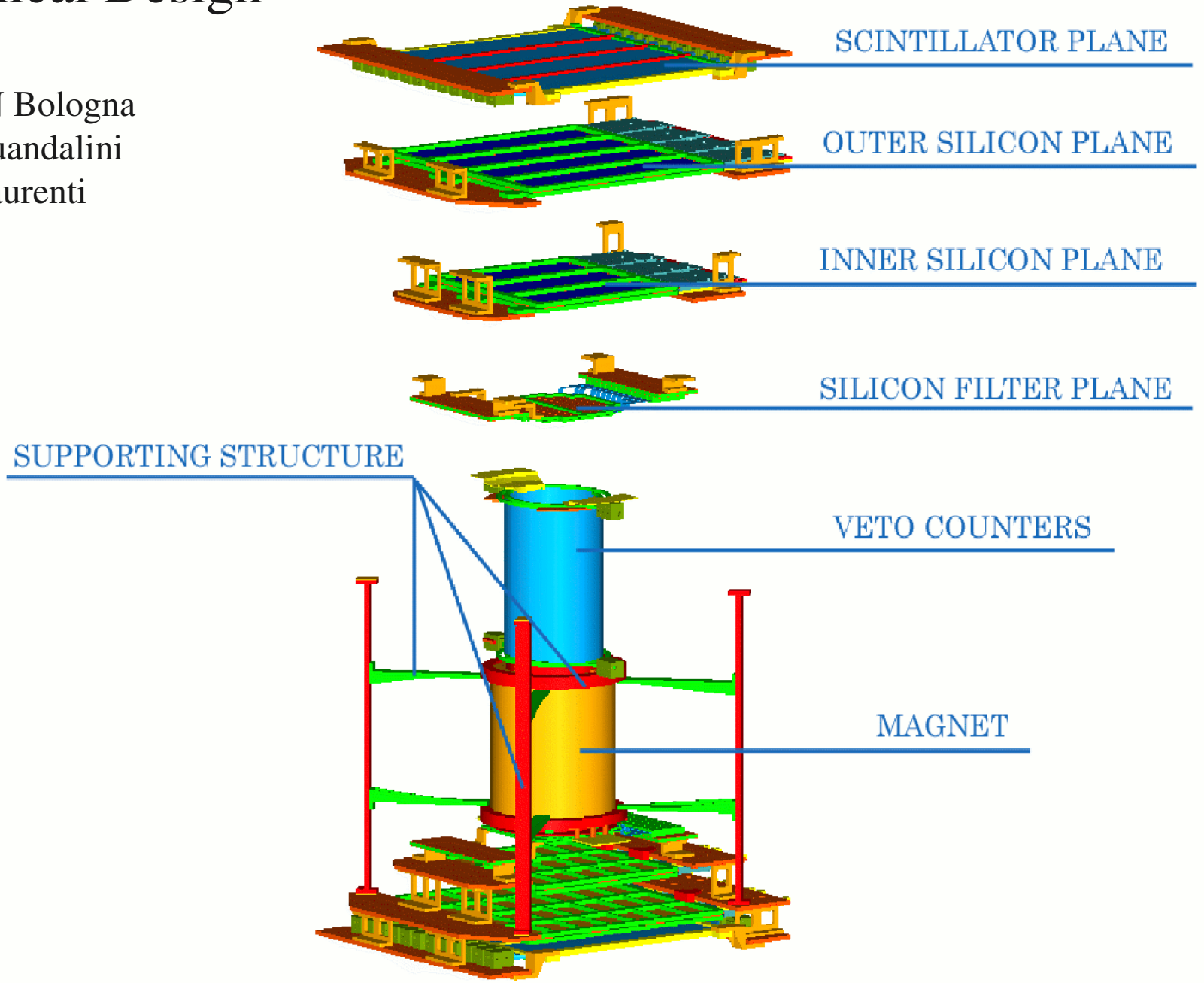

Mass and Power Estimates

conversions: **I AMS-02 T-Crate (24 TDRs) + cables = 14.5 kg**
1 AMS-02 T-Crate + 1 AMS-02 TPD = 84 W
1 AMS-02 TPD = 8 kg

TOF photo-multiplier mass / power: 20-25 g / 0.1- 0.5 W

	-------- acceptances --------					
magnet	**total**	**1-slit**	**2-slit**	**electronics**	**sub-total[1]**	**power[2]**
kg	*cm^2-sr*	*cm^2-sr*	*cm^2-sr*	*kg*	*kg*	*W*
5.0	**30**	**4.3**	**0.2**	**8.4**	**13.4**	**39.5**

[1]does not include detectors, Si frontend electronics

[2]includes 31.5 W for silicon detector readout and 8 W for the TOF PMs

Maximum Mass 15 kg **Maximum Power 25 W**

Data Rate Estimate

Estimated proton flux in the range 16-500 MeV based on the 2003 data of the omnidirectional MEPED of the NOAA 15 satellite, altitude 815 km (left); the estimated electron flux in the range 35-500 MeV, extrapolated from the 2003 data of the 0° MEPED (0.3-2.5 MeV) using an energy dependence of αE^{-3} (right).

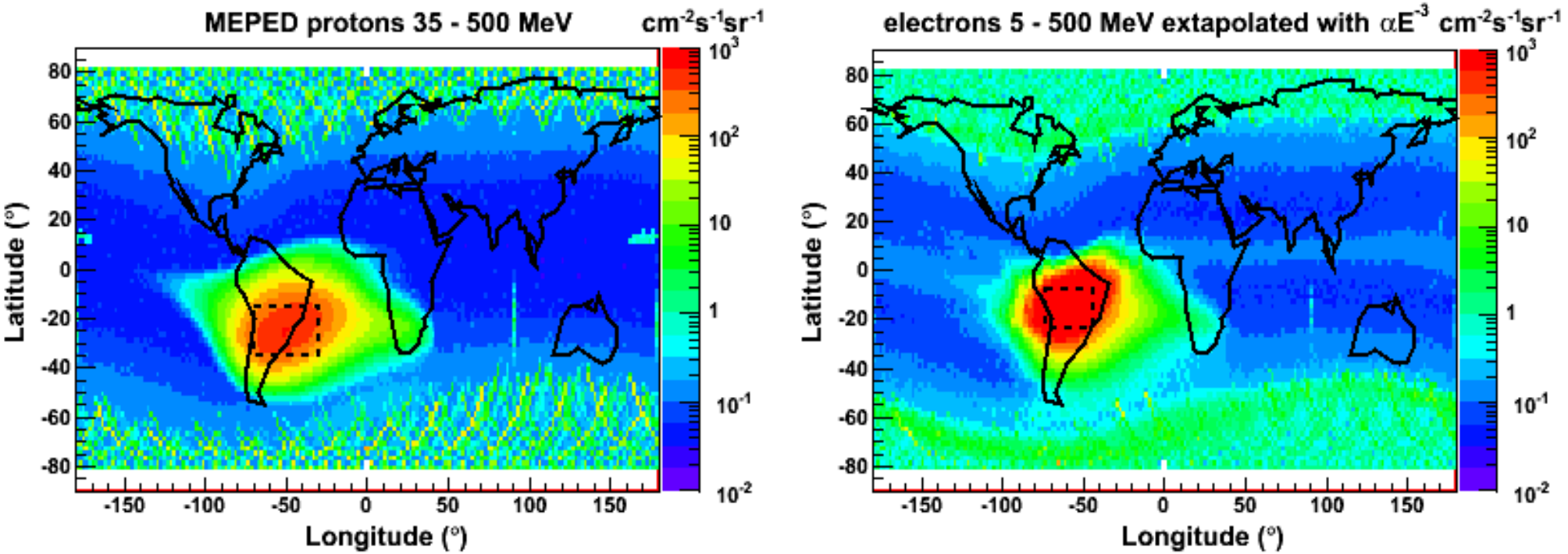

Average Flux, Event and Data Rates, and Daily Data Set Size

Geometric Acceptance 30 cm^2-sr

() values outside the SAA

particle	**flux** *cm^{-2}-sr^{-1}-s^{-1}*	**event rate** *s^{-1}*	**data rate** *bit-s^{-1}*	**total 24h** *bit*
electron	42 (16.5)	1260 (495)	575k (226k)	50G (20G)
proton	12 (7)	360 (210)	164k (96k)	14G (8.3G)
	Totals	**1.6k (0.7k)**	**0.74M (0.32M)**	**64G (28.3G)**

X-Band, Bit-rate 66Mbit/s, Daily Transmission Time 2000s, Capacity 132 Gbit/day

Similar estimate for LEPD (2.1 cm^2-sr, 30 Hz max. trigger rate) : 37 Gbit/day

Frascati BTF – 50 MeV electrons

Magnet and Upstream Detectors

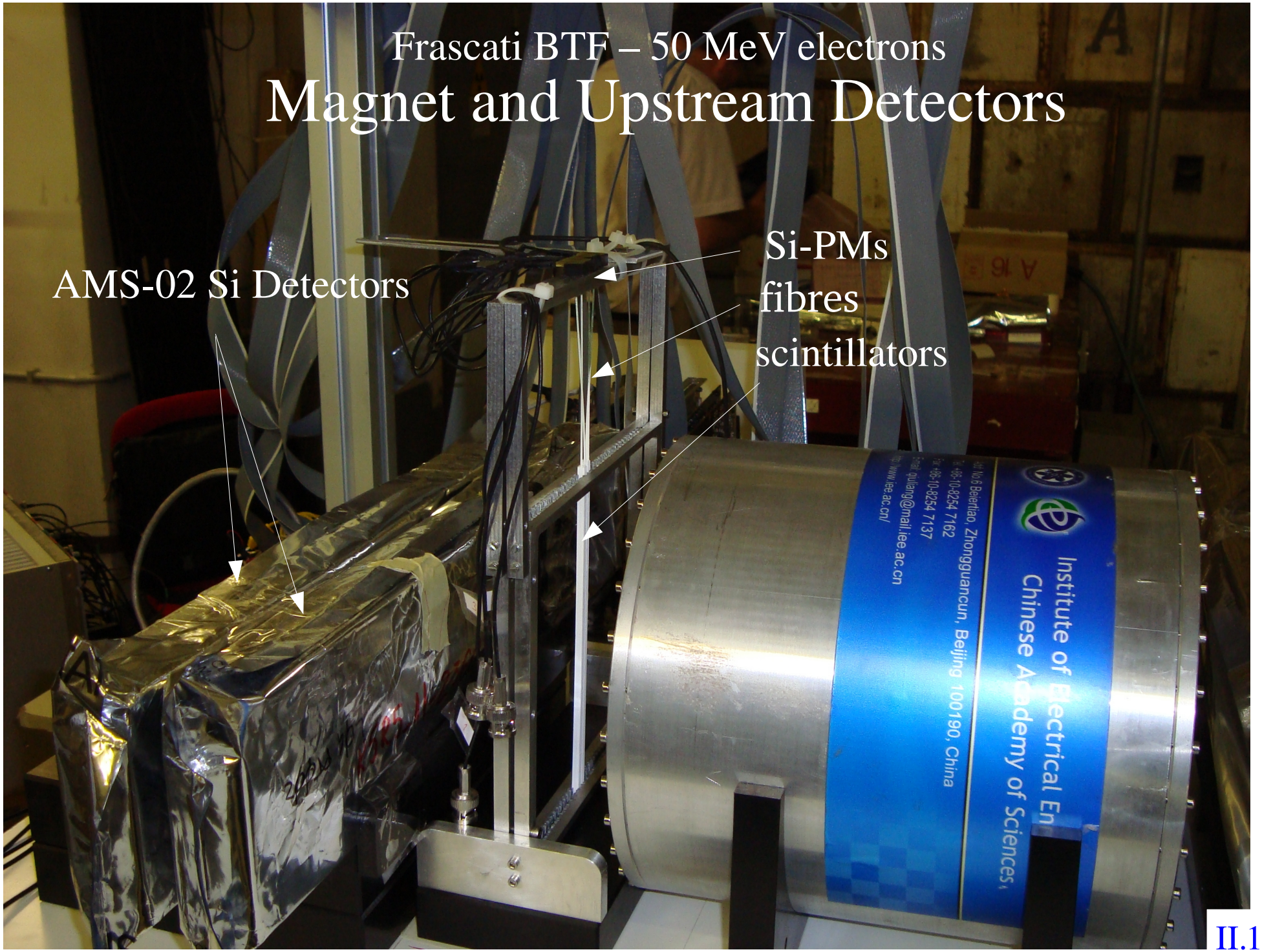

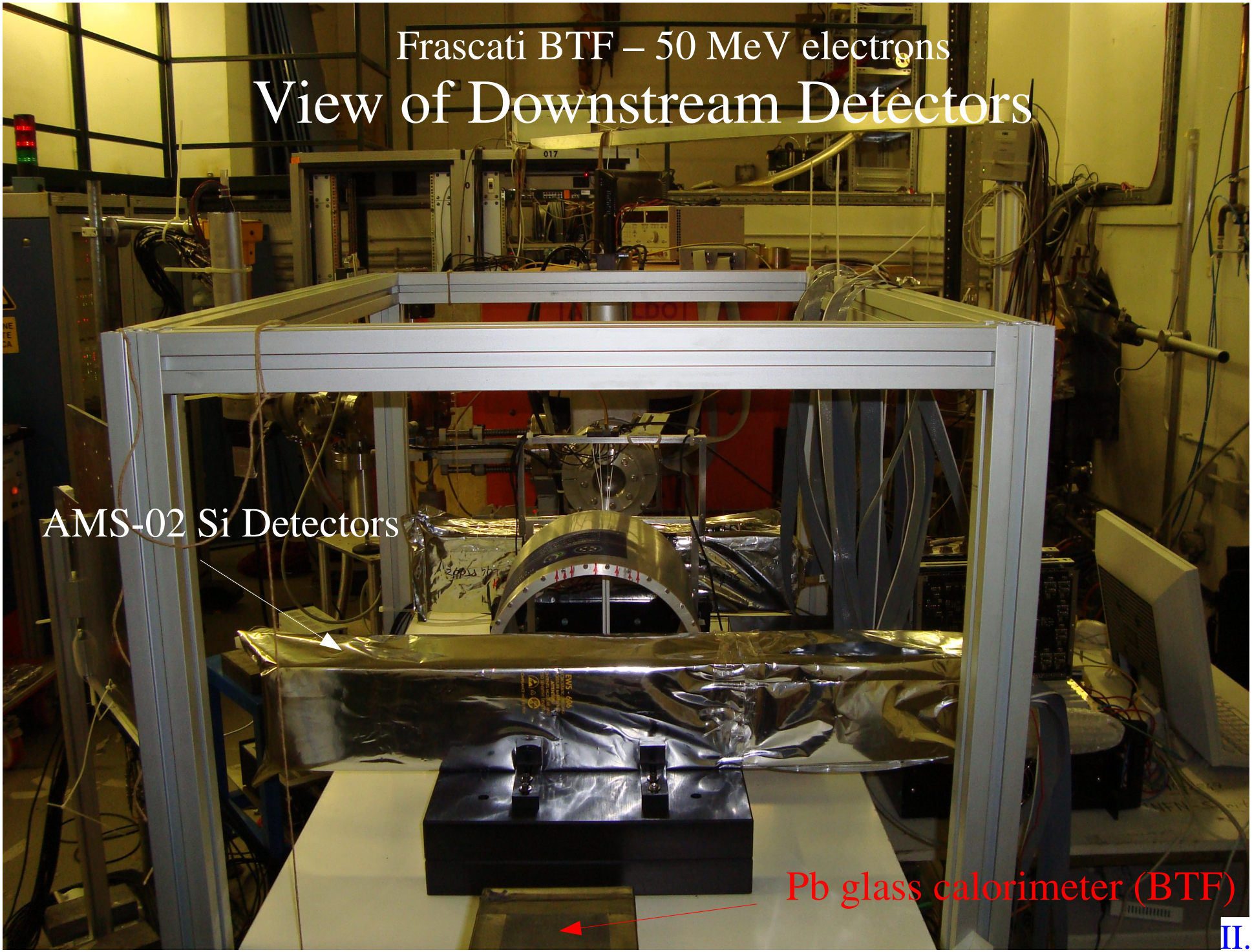
Frascati BTF – 50 MeV electrons
View of Downstream Detectors
AMS-02 Si Detectors
Pb glass calorimeter (BTF)

Reconstructed Beam Momentum (B=522G)

52.2 MeV/c Veto-OR of scintillator Si-PMs

Data

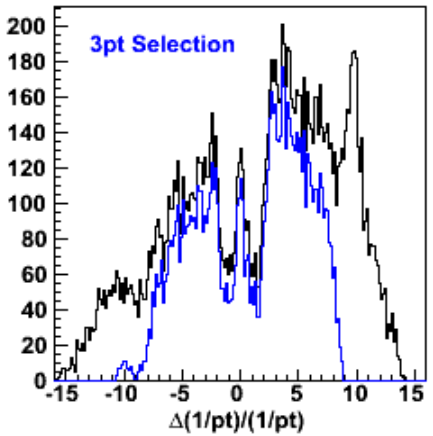

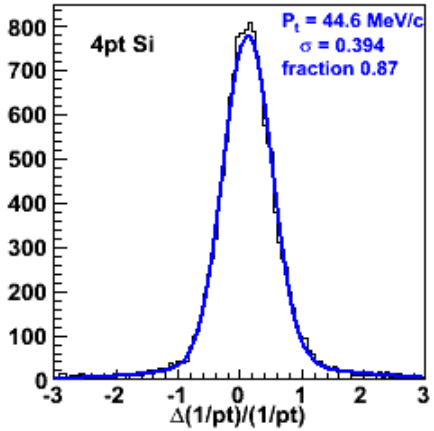

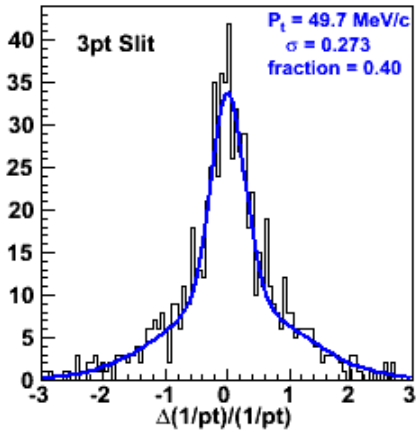

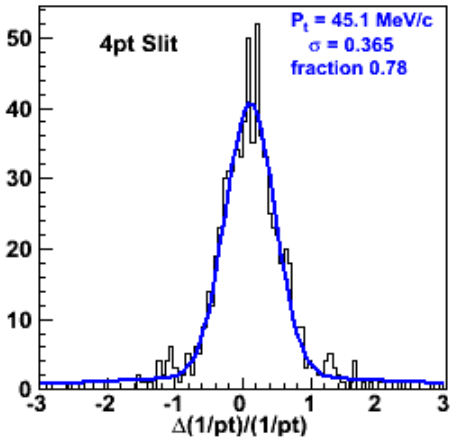

Simulation

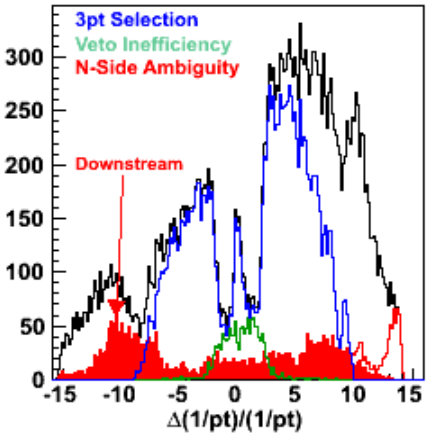

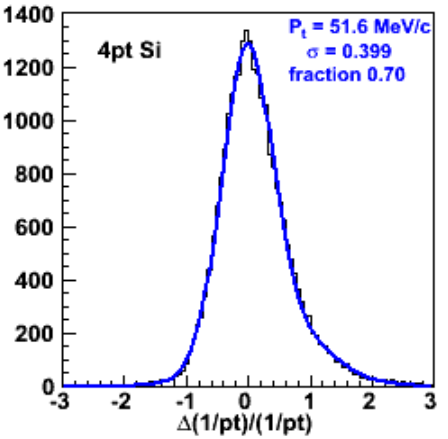

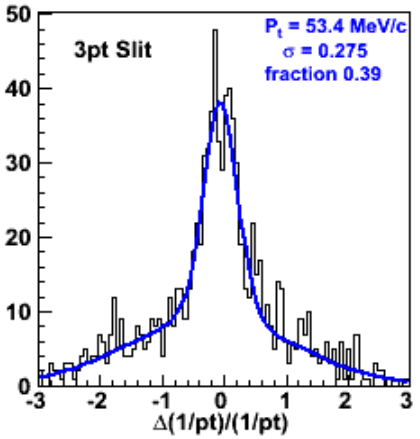

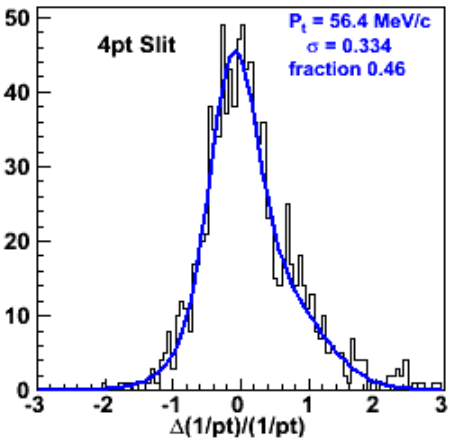

$\Rightarrow \Delta p/p = 25\%$

Aiglon-E

la version désaimantée

W.J. Burger
04.09.2013

PRIN05: Considerazioni per Il Rivelatore di Particella "L'Aiglon"

W.J. Burger, Perugia

Abstract

Electron and proton detection in the energy range from 1 MeV to 1 GeV has been studied with detector configurations based on momentum reconstruction and a total energy measurement. The expected angular resolution, which is provided by a tracking device common to the two types of detectors, is also reported. The acceptance is discussed in the context of a magnetic spectrometer.

The particle detector(s) determine the energy and direction (pitch angle) of the magnetically trapped electrons and protons encountered in the near-Earth orbit of the satellite. The energy resolutions obtained with momentum reconstruction and calorimetry have been evaluated with a Monte Carlo simulation. The detector configurations studied with Geant3 were: (1) a silicon tracker in a 1 kG field, (2) a silicon tracker (without magnetic field) and BaF_2 crystal calorimeter and (3) a scintillating-fiber tracker with the 1 kG field.

Radiation Yield

fraction of electron energy lost in *bremsstrahlung*.

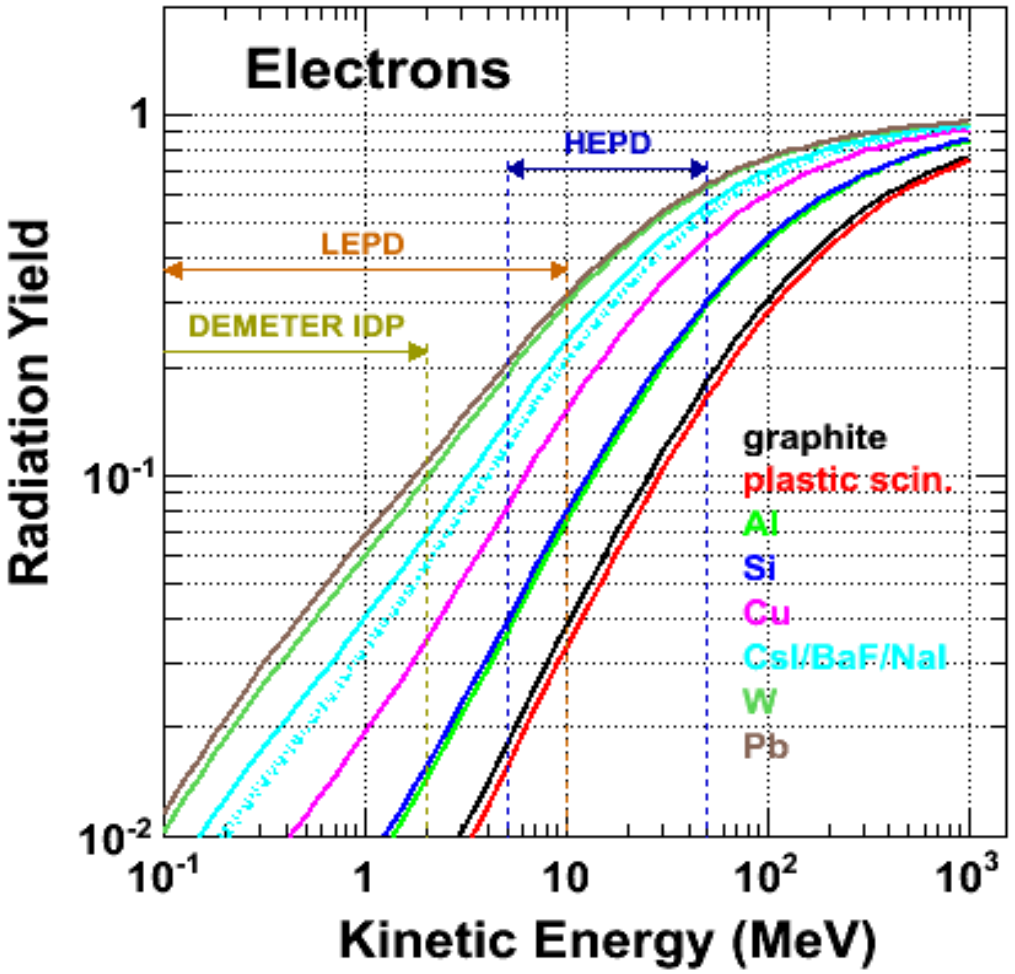

Aiglon-E

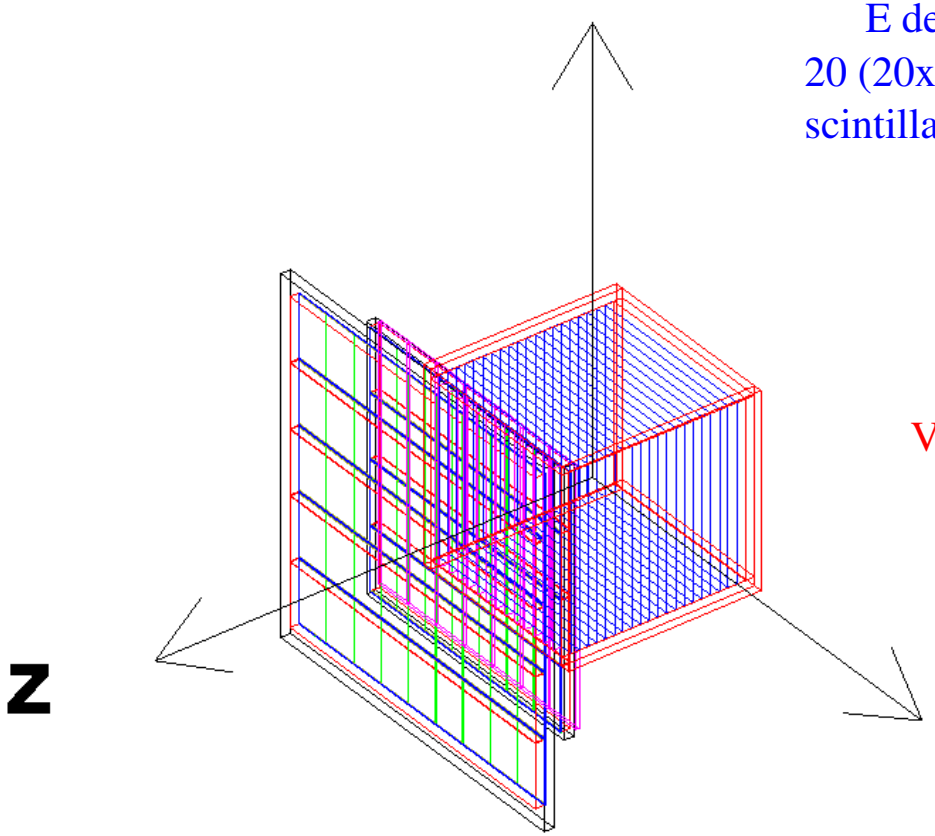
y
z
x

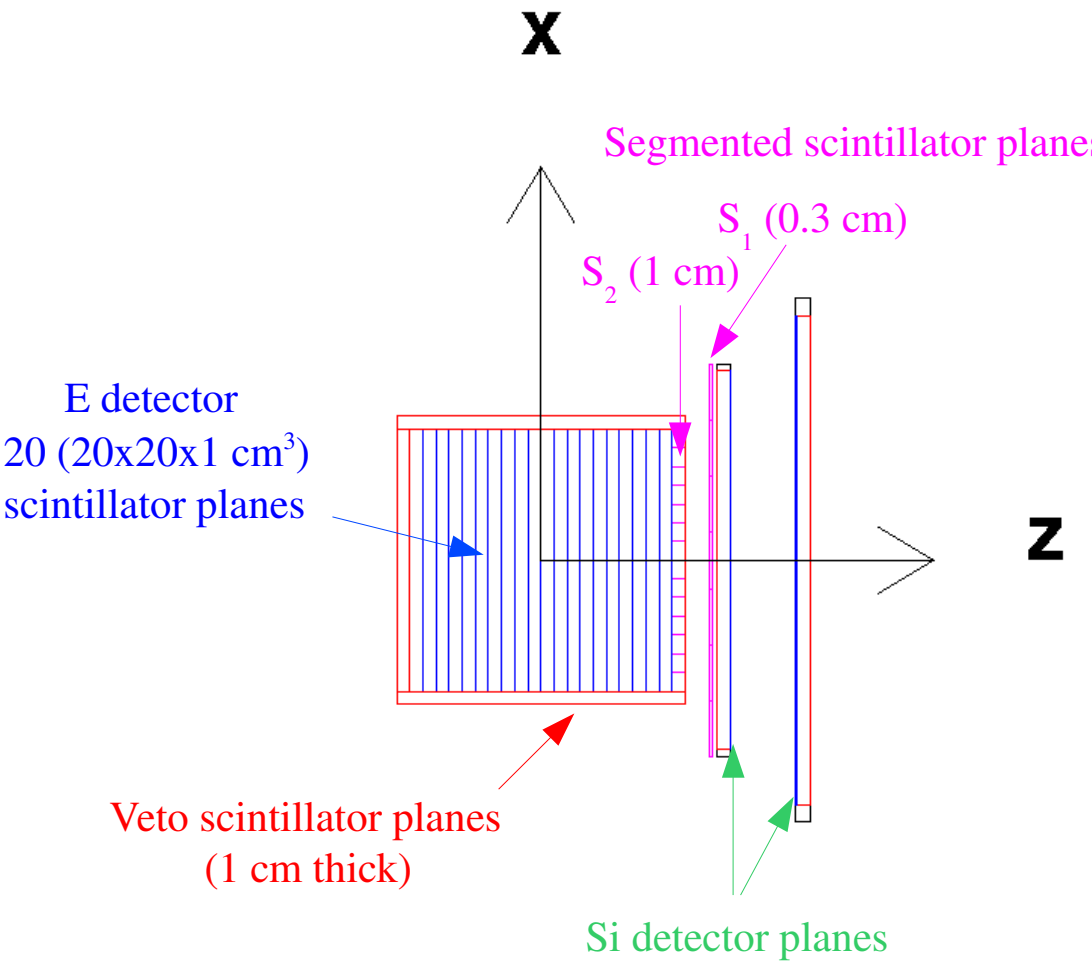
x
Segmented scintillator planes
S1 (0.3 cm)
S2 (1 cm)
E detector
20 (20x20x1 cm3)
scintillator planes
z
Veto scintillator planes
(1 cm thick)
Si detector planes

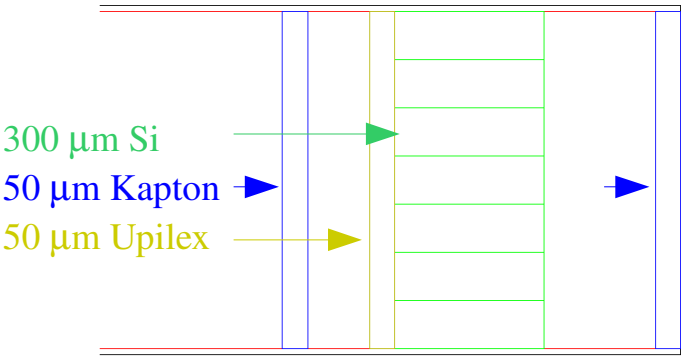
300 µm Si
50 µm Kapton
50 µm Upilex

The performance was studied with an event selection which requires a hit in the two scintillator planes S_1 and S_2 , both silicon tracker planes, and no hit in the veto planes recorded for the primary electrons.

Energy Measurement Electrons

Sum of ionisation energy losses recorded in S_1, S_2, Si tracker and E detector (scintillator)

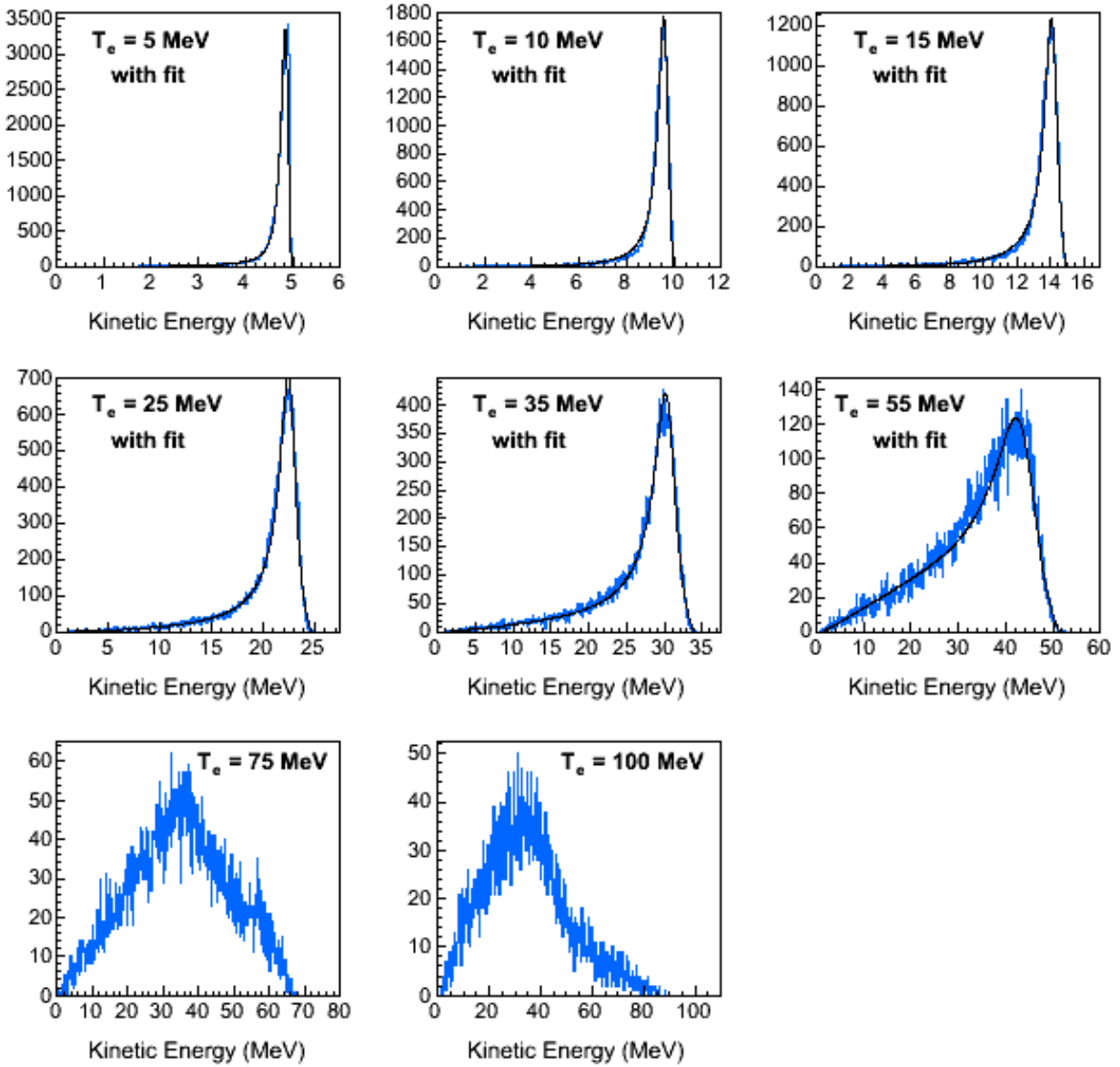

Energy Measurement Electrons

Sum of ionisation energy losses recorded in S_1, S_2, Si tracker and E detector (BaF_2)

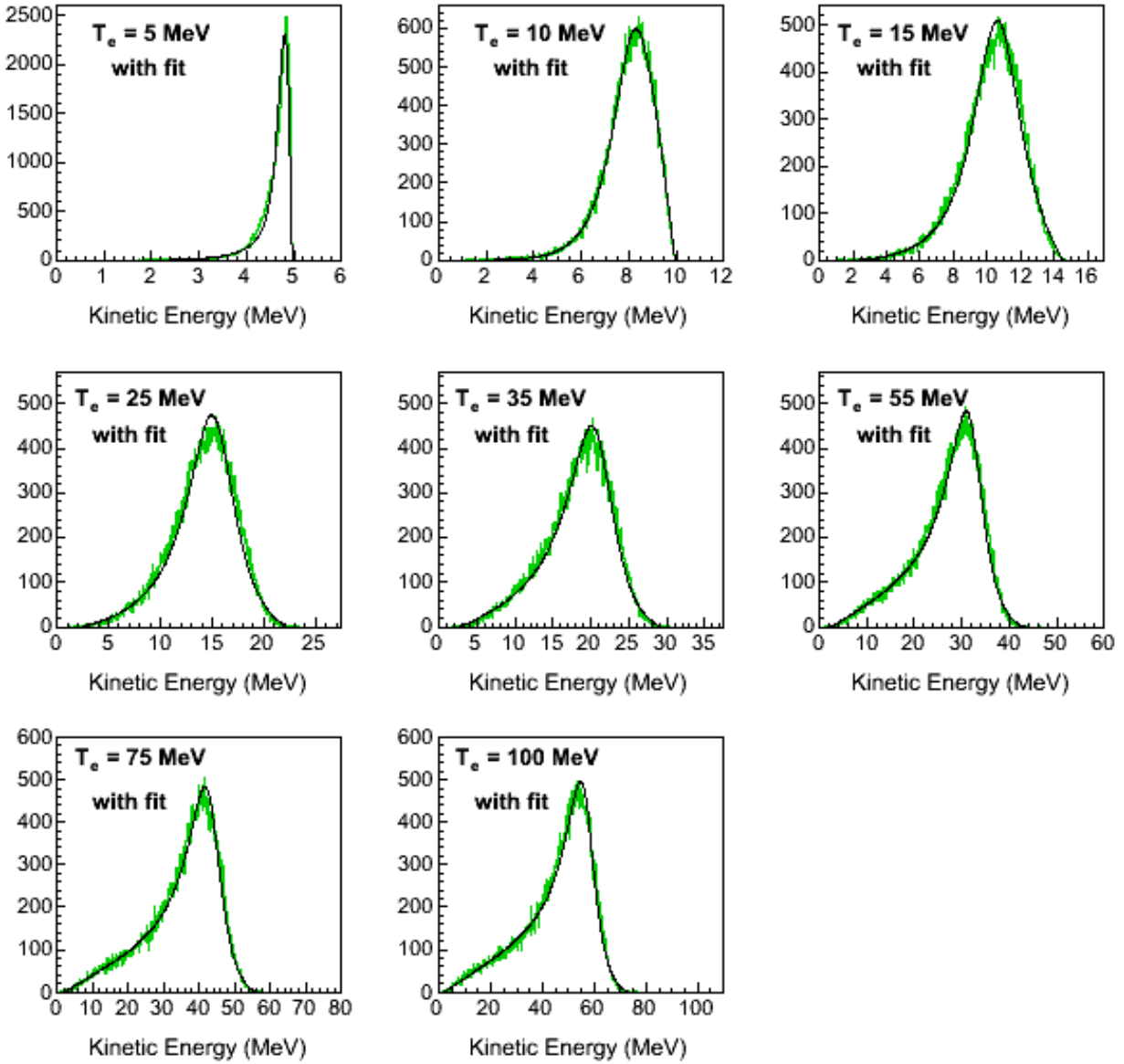

Kinetic Energy Peak Values and Distribution Widths Electrons

E detector volume of 20 x 20 x 20 cm^3

Scintillator			BaF2		
T_e	FWHM	T_{fit}	T_e	FWHM	T_{fit}
MeV			MeV		
5	0.2	4.8	5	0.3	4.8
10	0.5	9.6	10	2.0	8.2
15	1.0	14.1	15	3.1	10.5
25	2.0	22.5	25	7.9	14.5
35	3.7	30.1	35	8.9	19.0
55	14.0	41.7	55	12.5	27.9
			75	13.2	41.1
			100	16.9	54.0

Pitch Angle Resolution Electrons

For different thickness silicon detectors, including 100 μm for the Kapton EM shield and the 50 μm thick Upilex cable

	Silicon detector thickness (μm)		
T_e (MeV)	300	200	65
5	8.3°	7.0°	5.3°
10	4.9°	3.7°	2.8°
15	3.0°	2.5°	1.8°

Pitch Angle Acceptance Electrons

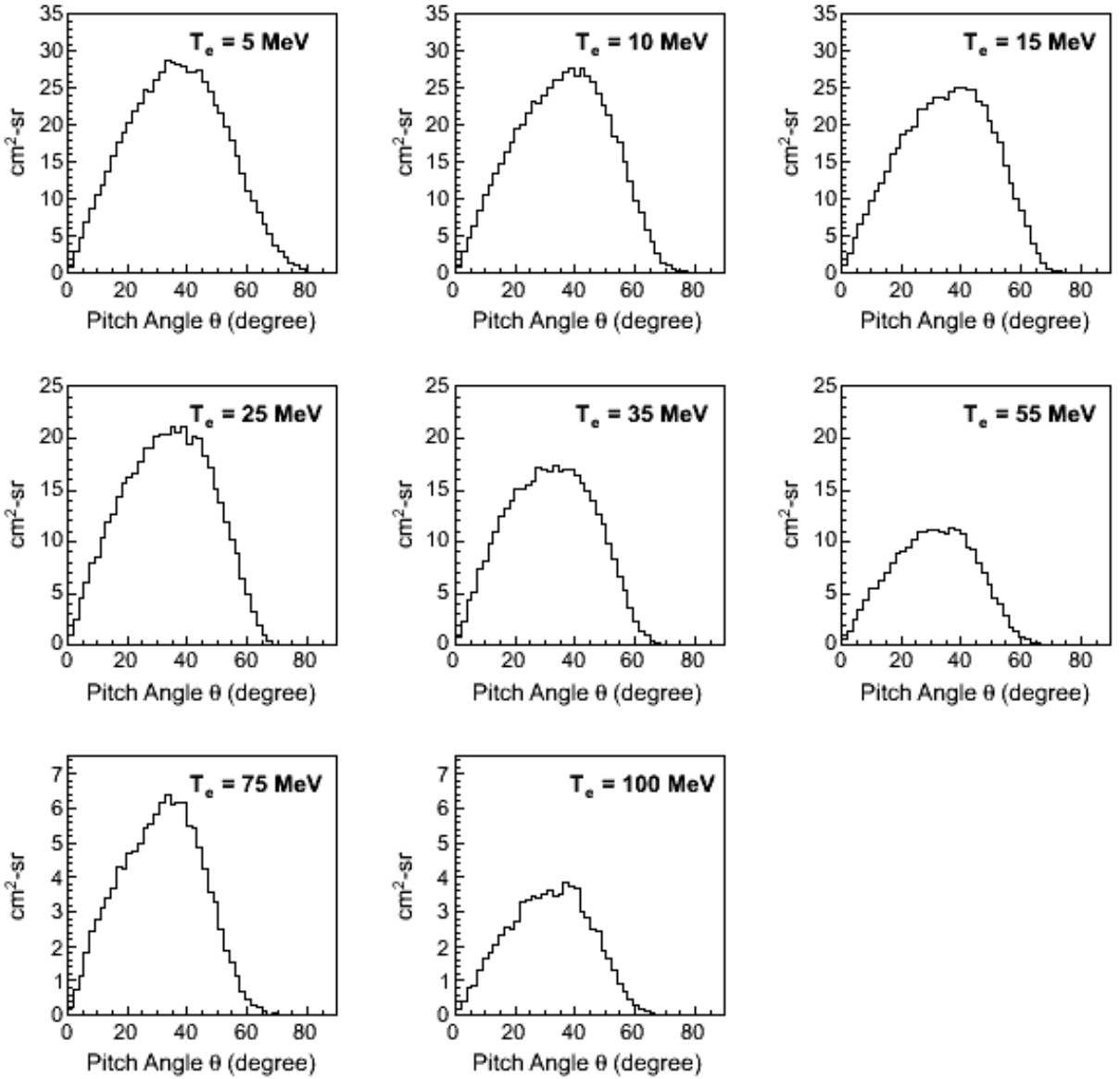

Angle Integrated (Total) Acceptance Electrons

for the two 20 x 20 x 20 cm^3 E detectors

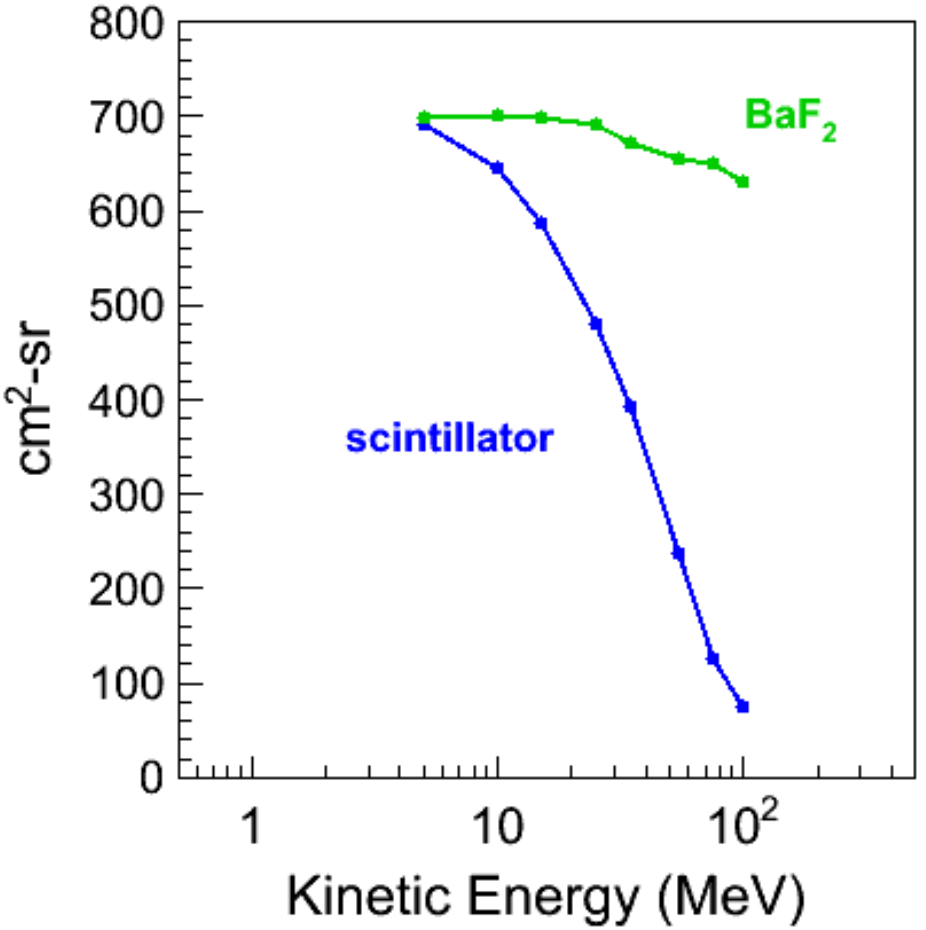

The electrons and protons are distinguished by using their velocity in the kinetic energy 1-500 MeV. The difference in β affect their time-of-flight, energy loss and range

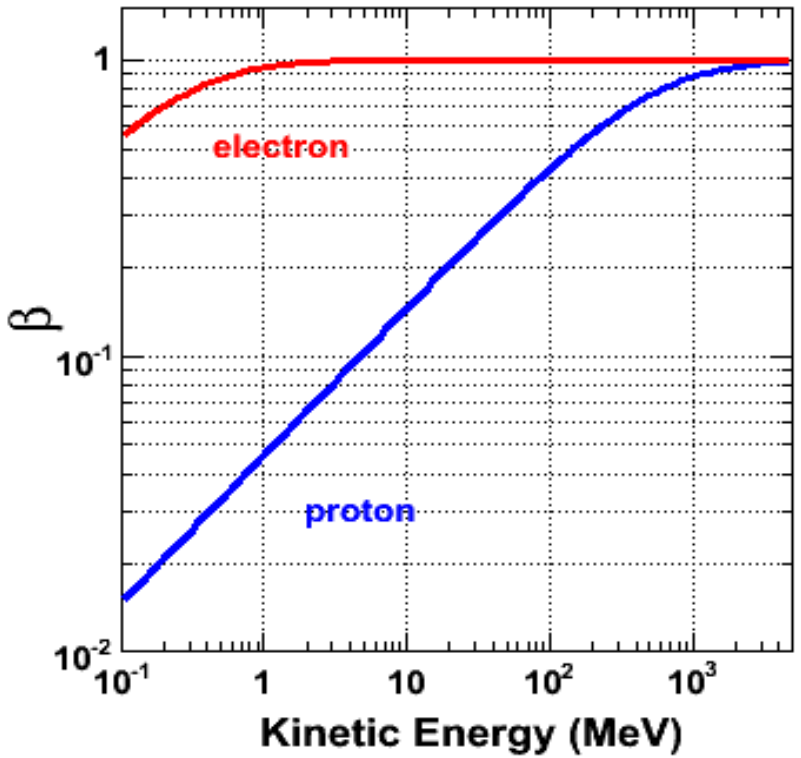

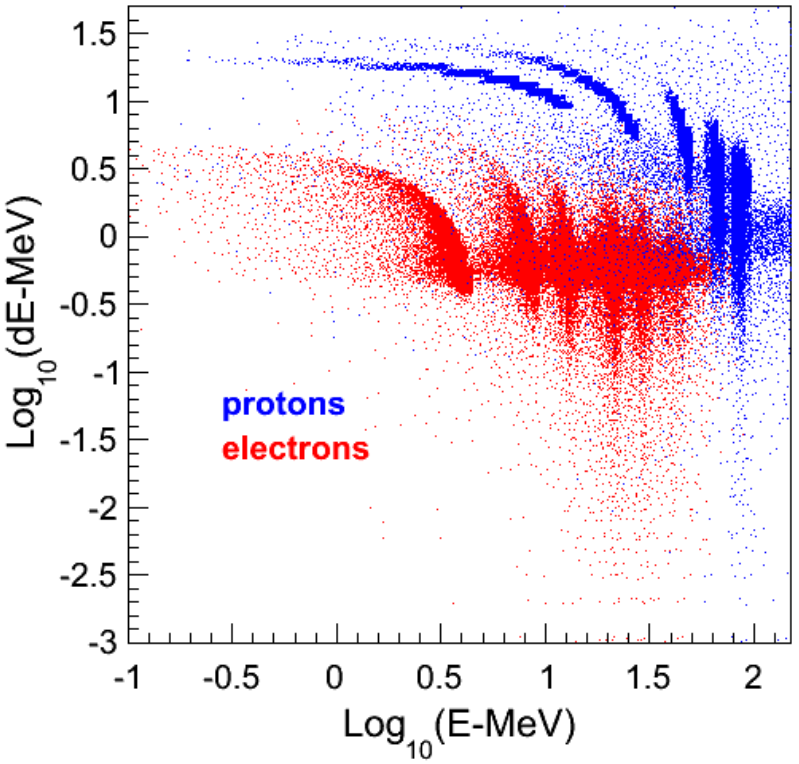

The electrons and non-relativistic protons in the kinetic energy range, 1-100 MeV, may be distinguished by dE/dx and range.

55 MeV electrons

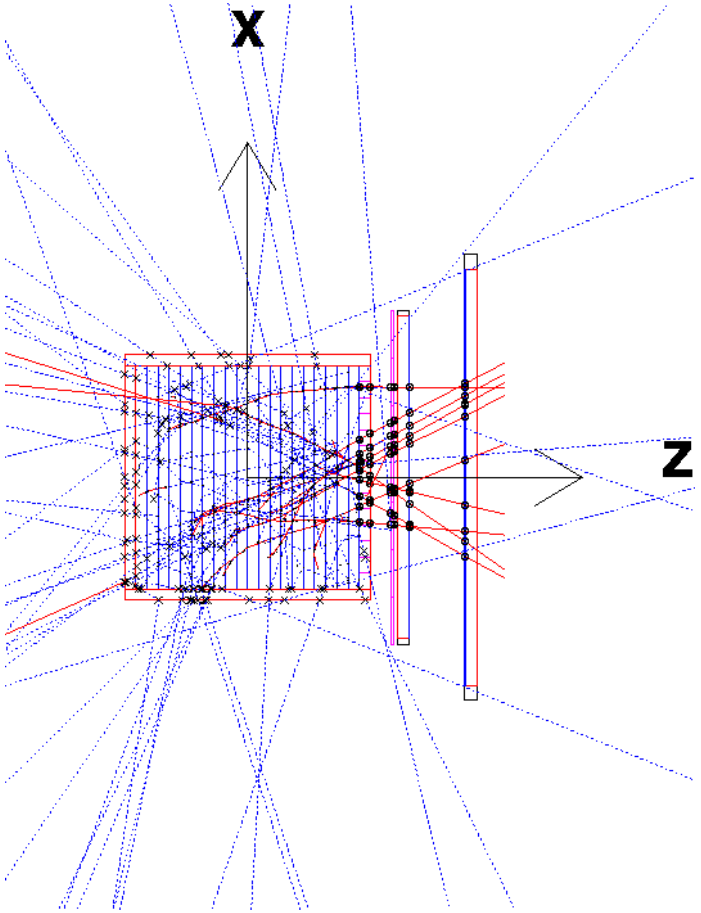

55 MeV protons

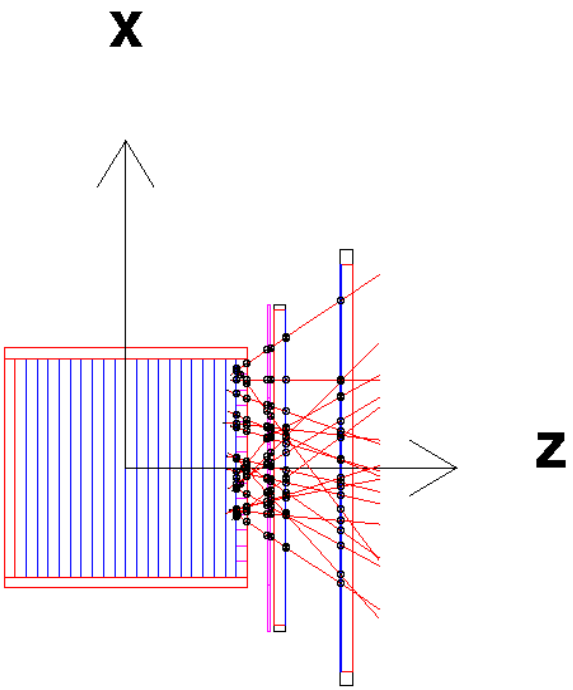

Flux Estimates for Background Determination

A.M. Galper, Erice, Italy, 23 October 2012

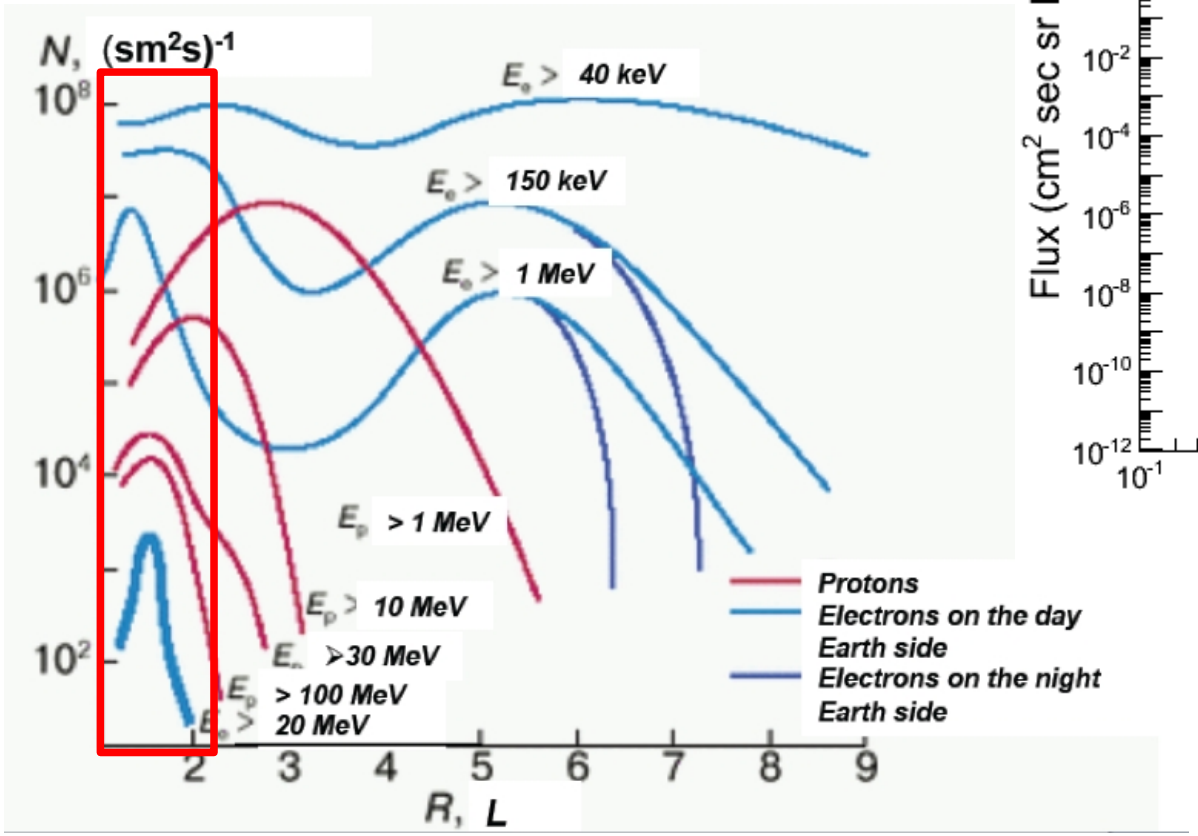

Electrons

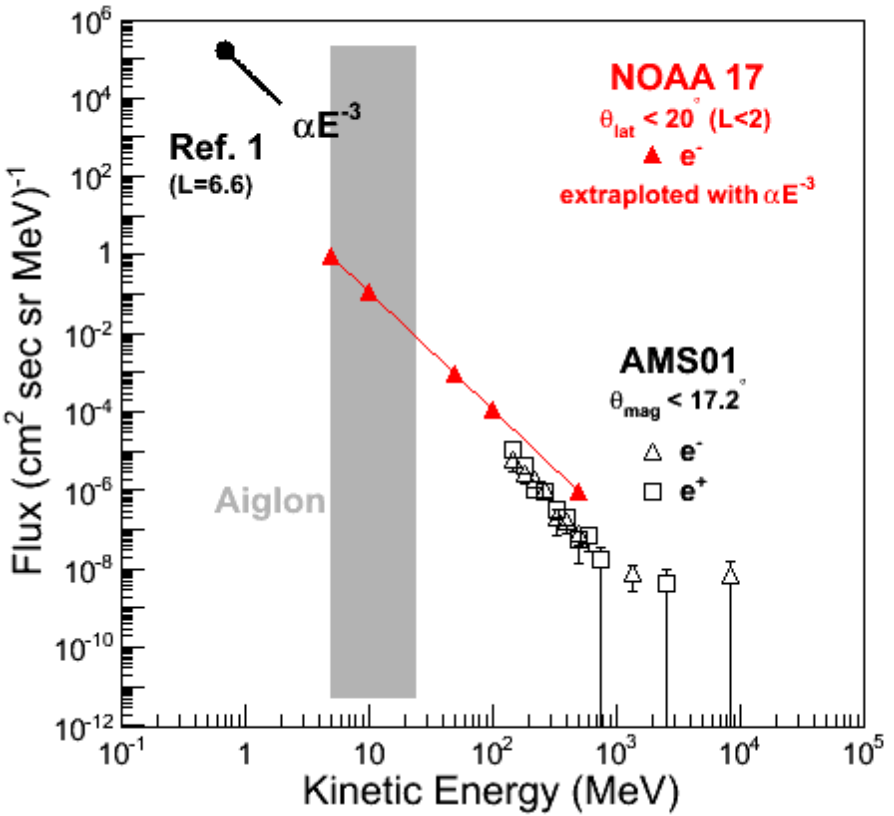

Mass

The mass of the 22 x 22 x 22 cm^3 scintillator E detector, including the veto planes and S_2 scintillator is 11 kg.

The mass of a 20 x 20 x 20 cm^3 BaF_2 E detector is 40 kg.

Power and mass limits for the HEPD are 25 W and 15 kg.

Current Status

The energy resolution performance of Aiglon-E (5-10 % between 5-35 MeV) is comparable to the version magnetic spectrometer.

The angular resolution is improved with the sacrifice of the TOF measure, but *a priori,* performace for proton/electron separation depends on β, common to the different measurement techniques.

The angular acceptance is very good. A reduction of the dimensions of the calormeter affects both the angular and energy acceptances.

The performance for protons has not be studied.

ARINA instrument

On the basis of multilayer scintillation detector.
Acceptance of ARINA 10-50 times higher than acceptance of instruments, used in earlier experiments for similar studies.

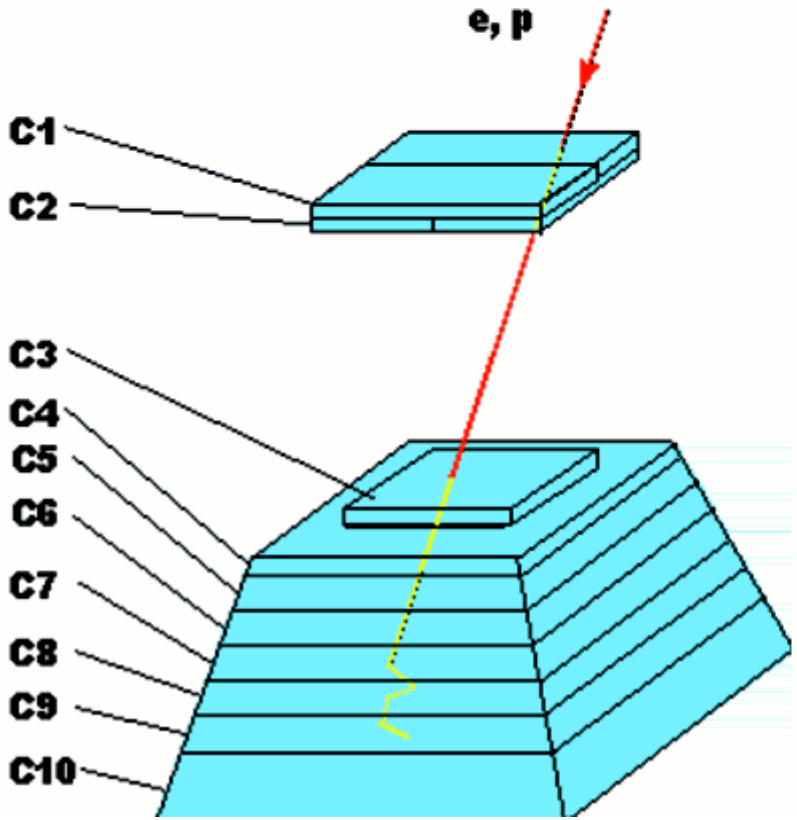

Acceptance		10 sm^2sr
Aperture		±30 degrees
Energy range	protons	30 – 100 MeV
	electrons	3 – 30 MeV
Energy resolution	protons	10%
	electrons	15%
Time resolution		100 ns
Mass		8,6 kg
Power consumption		13,5 W

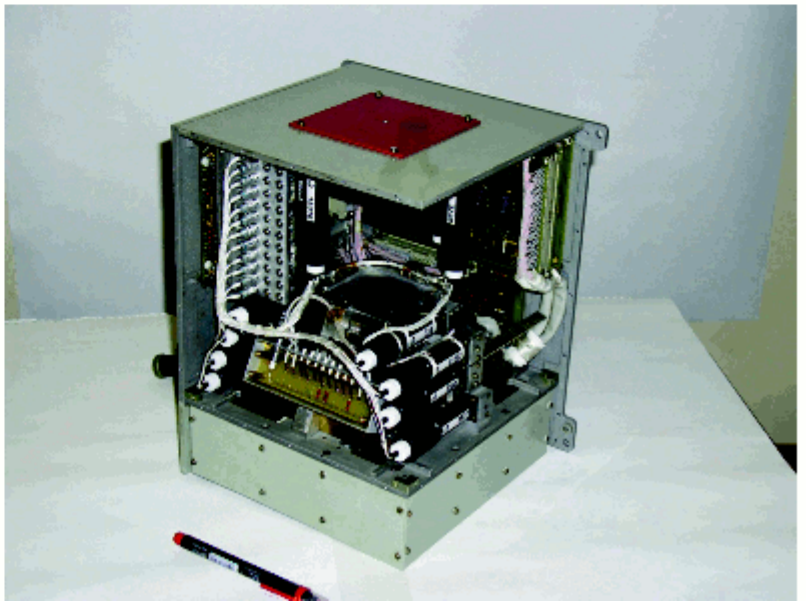

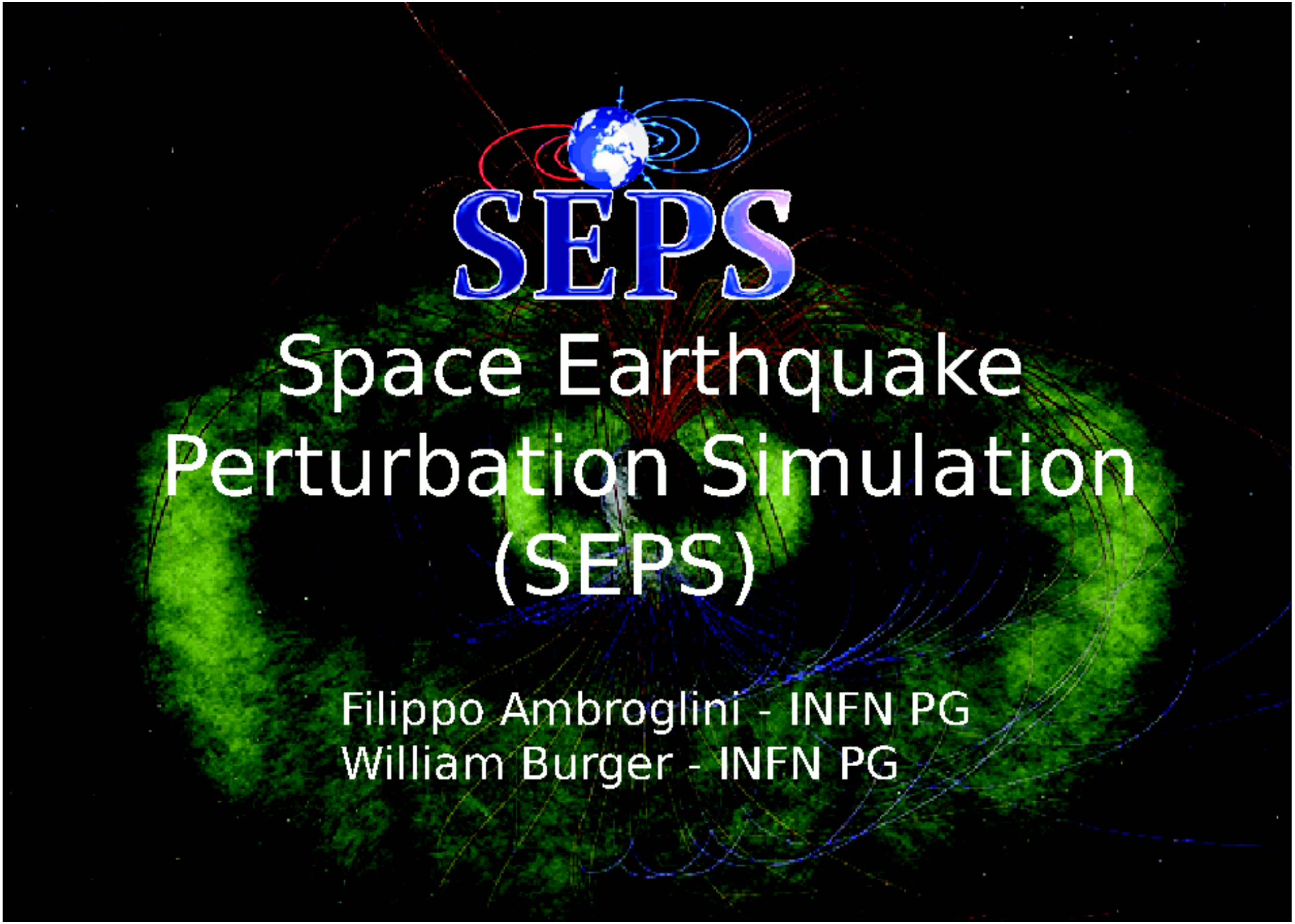
SEPS
Space Earthquake
Perturbation Simulation
(SEPS)
Filippo Ambroglini - INFN PG
William Burger - INFN PG

SEPS

A simulation code based on Geant4 and the PLANETOCOSMICS application that allow to simulate the interaction of the EM perturbation with the particle entrapped in the magnetosphere on a track by track basis.

IGRF model is used for the Earth's internal field. The external field may be added by choosing among the available Tsyganenko models.

The NRLMSISE00 model is used for the Earth's atmosphere.

AE8 (MIN, MAX, MINESA) particle flux model is used to define the kinematics of the particles

Two Approaches in the Simulaton

Start at the epicenter

- modelisation of the wave-particle interaction with the inner radiation belt particles
- study the optimal location of the satellite with respect to the epicenter location

Start at the observed site of the particle burst

- check the compatible of the observation with the site of the time-correlated earthquake (back trace)
- determine if the observed electrons occupy a stable drift shell (forward trace)

The 25 PB-EQ events in the ΔT = -1.25 h correlation peak of the NOAA POES analysis

PB o EQ •

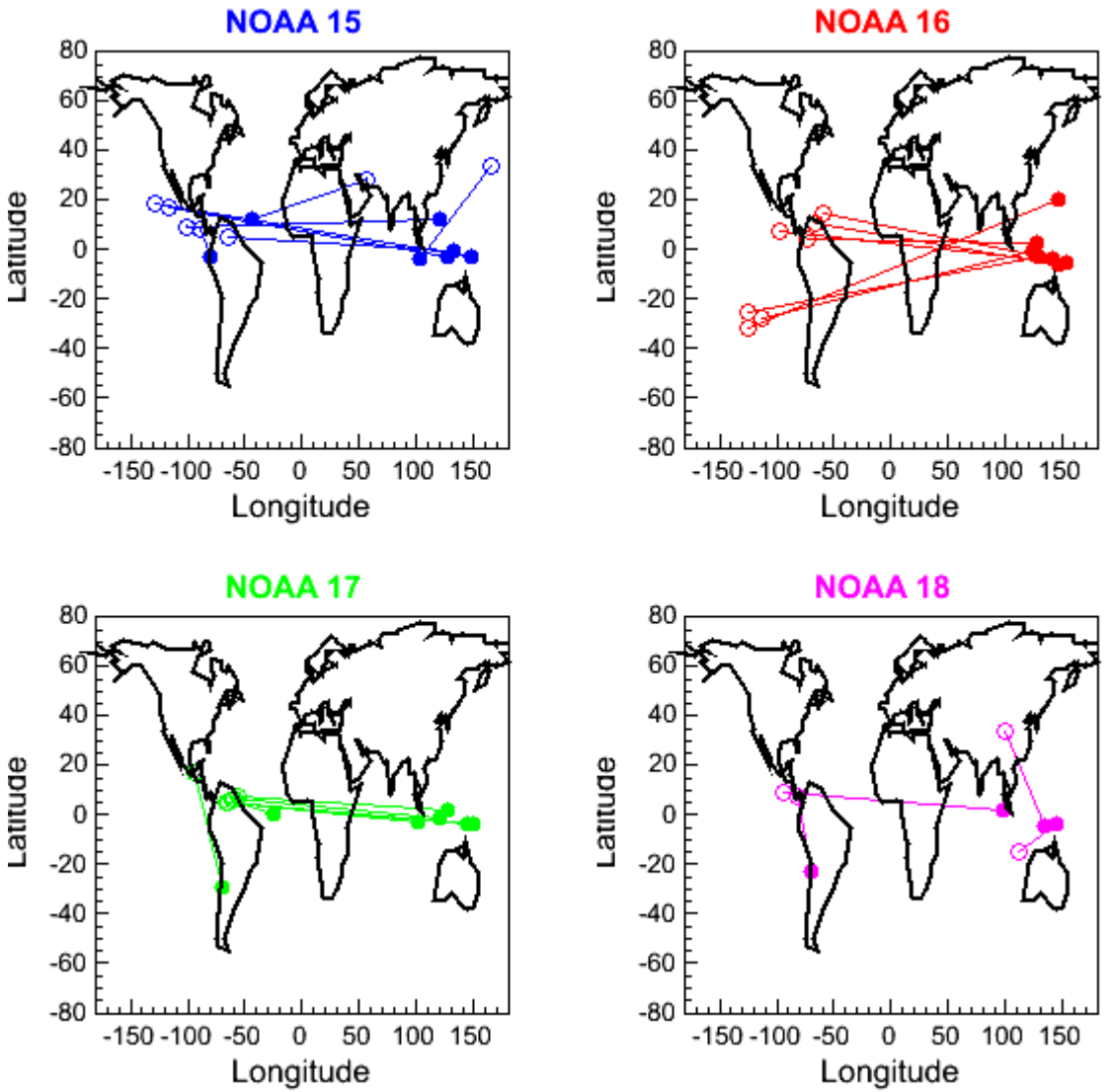

Back-Trace Analysis of POES Event

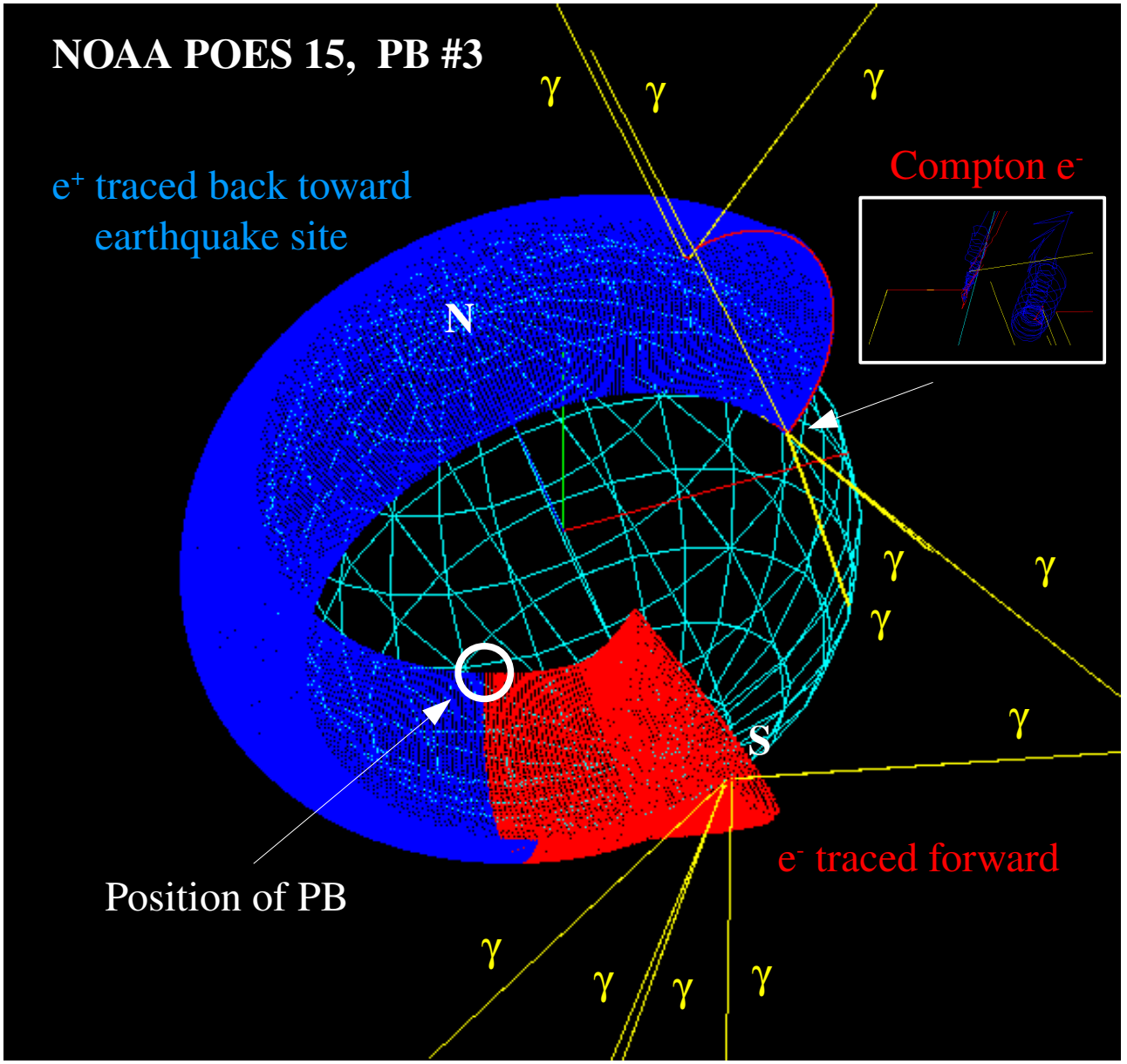

NOAA POES 15, PB #3

Positron back traced from the observation point (▼) is compatible with the earth-quake location (▲). Neither the positron nor the electron make a complete revolution around the Earth. an $e^{\pm}$ pair created in the atmosphere is visible at 50^{O} longitude.

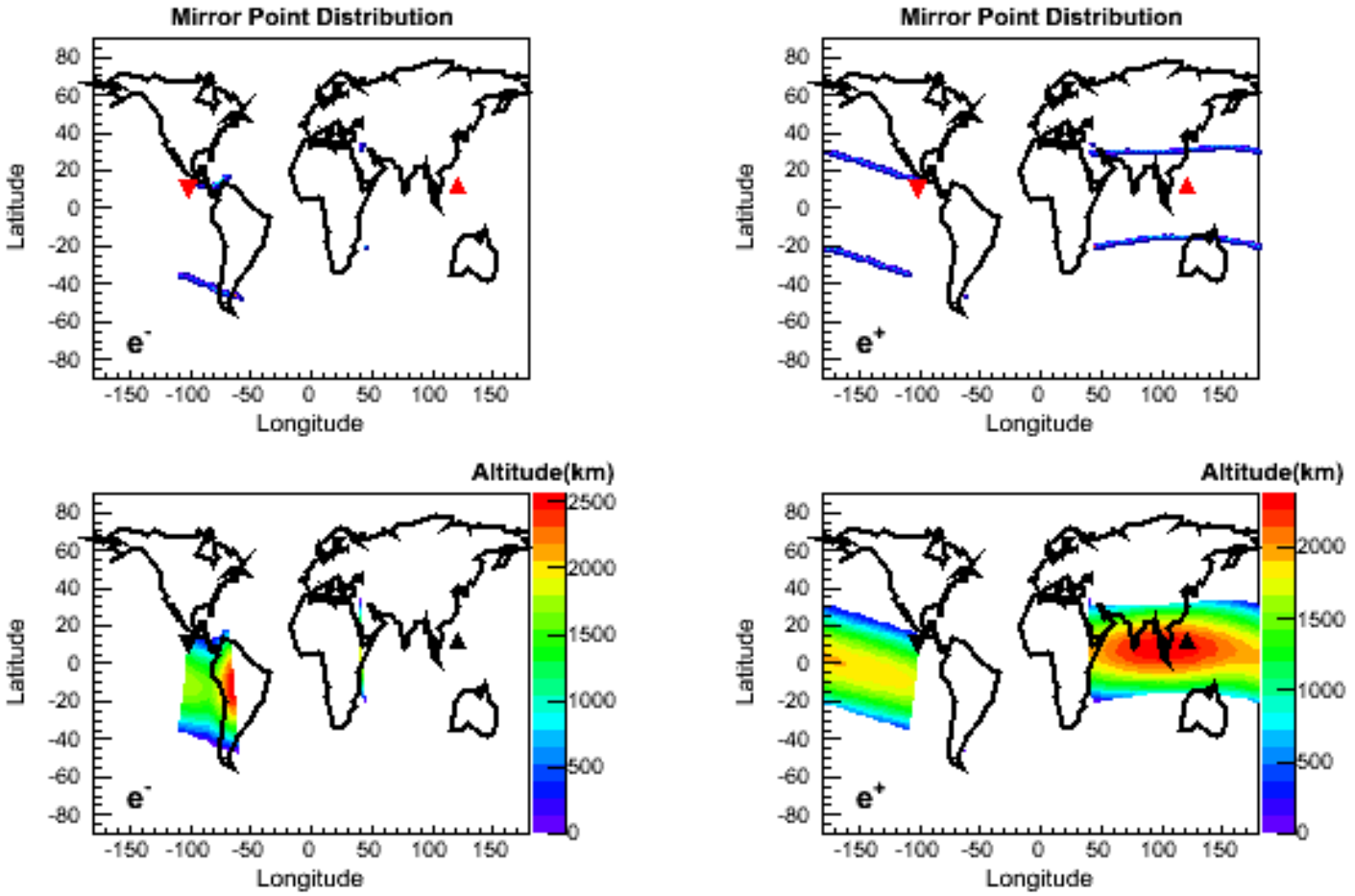

NOAA POES 17, PB #18

Positron back traced from the observation point (▼) is compatible with the earthquake location (▲). The trajectories of the observed electron and back traced positron appear to be stable, i.e closed trajectory around the Earth.

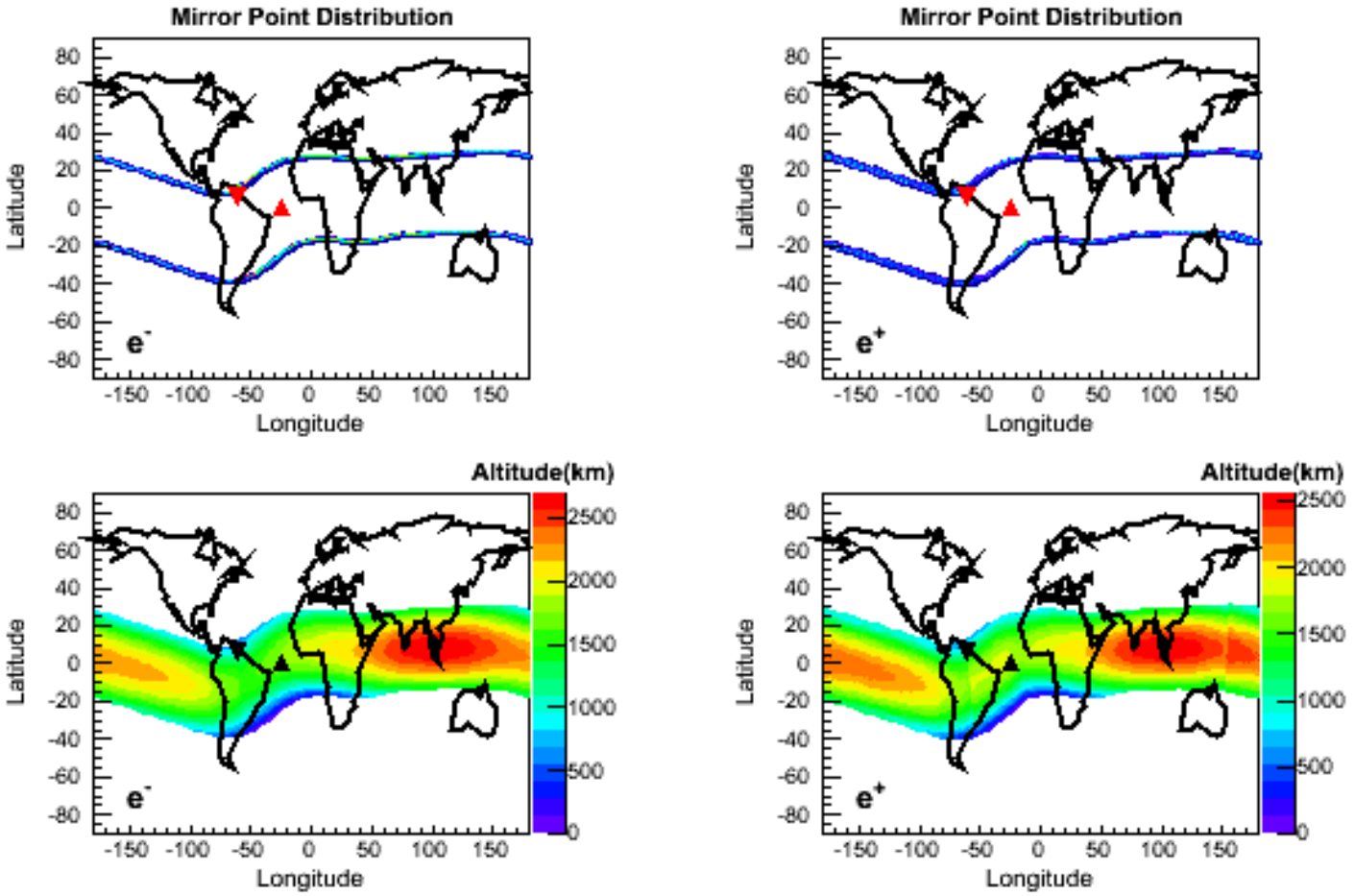

NOAA POES MEDPED
Electron Telescope

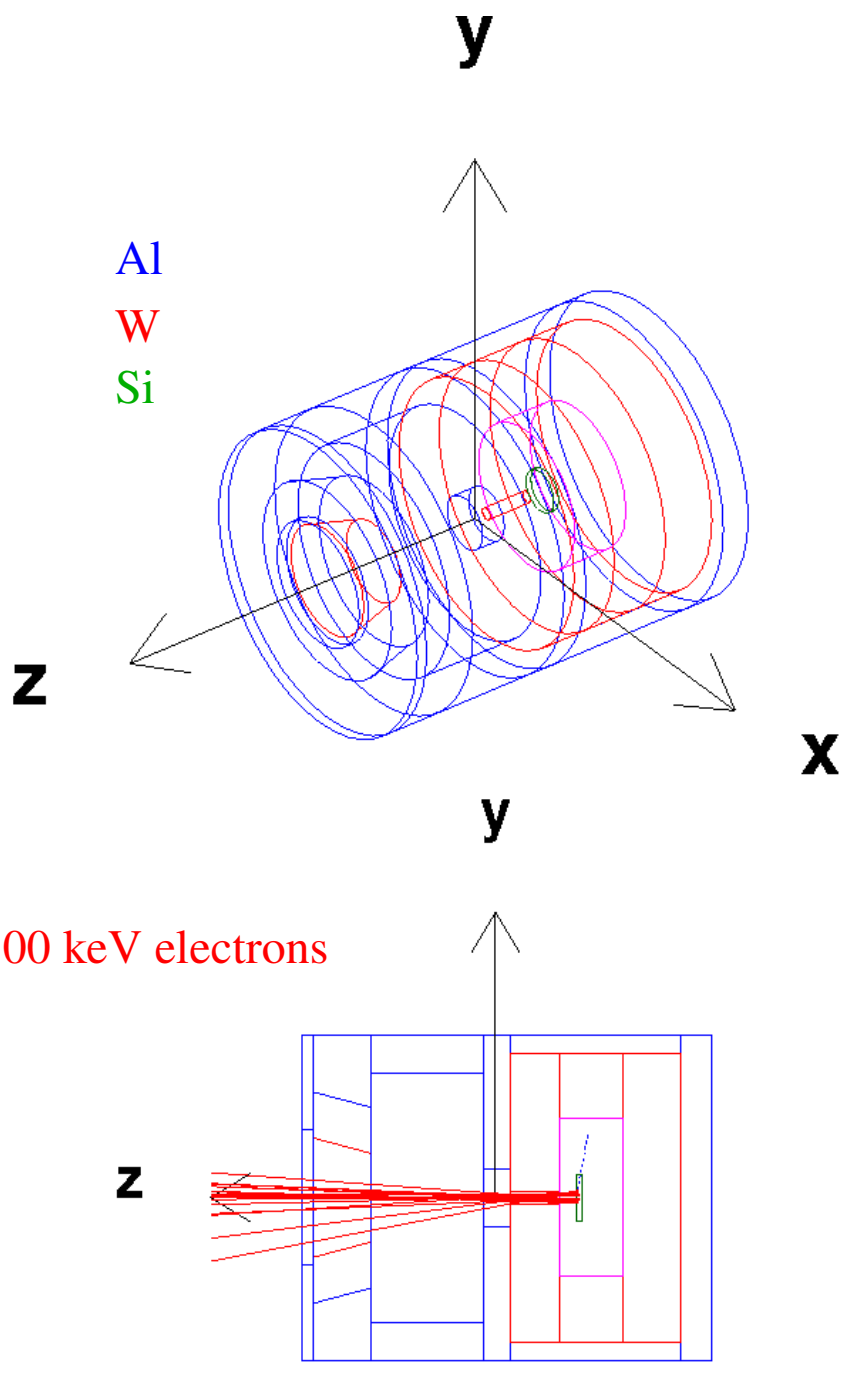

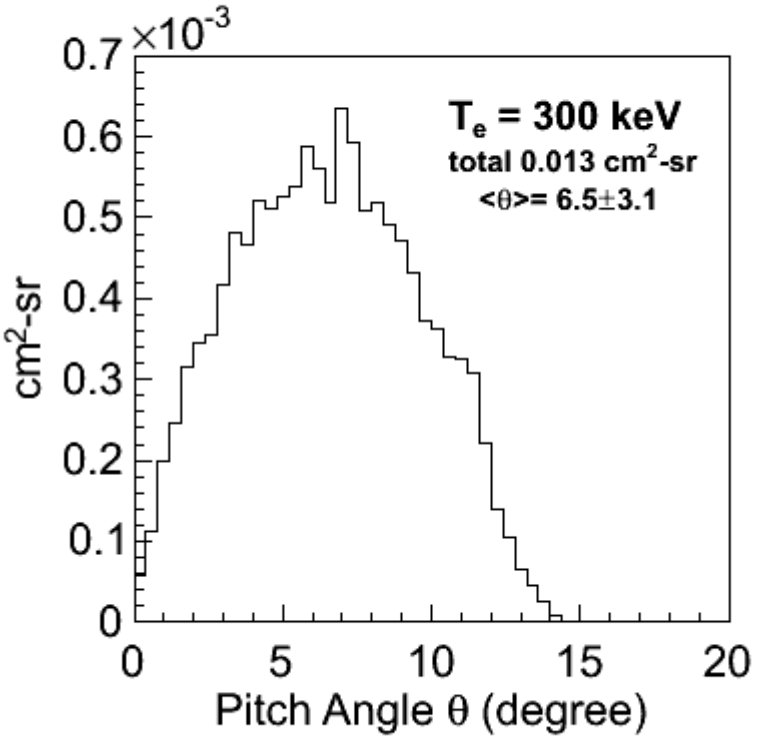

Back-Trace Analysis of POES Events

Inputs: the latitude, longitude and altitude of the satellite at the observation point and the field-of-view direction with respect to the local field line (local pitch angle).

First Conclusion

The analysis of the NOAA POES data indicates the importance of the local pitch angle.